

POLITECNICO DI TORINO

Corso di Laurea Magistrale in Ingegneria Aerospaziale

Master Degree Thesis

**Numerical Investigation on
Aerodynamic Stability
Derivatives of Earth Re-entry
Capsules**



**POLITECNICO
DI TORINO**

Supervisor:

Prof. Domenic D'Ambrosio

Candidate:

Chiara Ravera

s227242

**Supervisors in
Thales Alenia Space Italia**

Ing. Cosimo Chiarelli
Ing. Vincenzo Mareschi

March 2018

To V.,
"I don't know where I'm going,
but I promise it won't be boring."
(David Bowie)

Summary

Since the beginning of the space exploration era, when came the need to safely return humans and vehicles back to Earth, the studies on reentry phases, procedures and orbits saw their birth. Along with these, seemed clear that one aspect that really affected the success of those operations was stability, particularly in its dynamic meaning. This issue carries many difficulties for what concerns its formulation, evaluation and computation, since there are various approaches to this topic, and no univoque definition of dynamic derivatives seem to be existing, since many and different assumptions can be made.

The aim of this thesis is to identify a trustful model to rely on to get realistic predictions on a reentry capsule stability in terms of static and dynamic pitching moment coefficients.

First of all, a capsule is chosen for the following analyses (Hayabusa) and the flow conditions are established. In fact, thermodynamics and aerodynamics result strongly affected by altitude and state variables, so, to better understand the phenomenology, it is important to set those conditions, that will be further used as boundary/initial conditions. The chosen case is a subsonic one, which is very simplifying due to the avoidance of shock fitting need. Along with this assumption, only an axisymmetric geometry and only a motion on the plane of simmetry are considered.

Analyses for stability are performed with Numeca suite (composed as *flow solver: FINE/TurboTM* and *grid generator: IGGTM*) taking into account different settings of the capsule at different angles of attack, both in static and dynamic computations. In the latter, forced oscillation technique is employed to pursue the goal: a sinusoidal motion in pitching angle is applied to the solid boundaries while forces and pitching moment are monitored, to let then extract dynamic stability coefficients via an apposite Matlab code that compares two different approaches of the ones existing and presented in literature.

These results are then compared to an available database present in literature, based on the experiments conducted by Hiraki et al., and conclusions are extracted.

Since the basic assumptions and working conditions are quite restrictive and simplifying, limitations and future works for this thesis are then presented: the

aim of the project was not to get precise results, but was instead to find a good and improvable method to get reliable analyses and values.

Sommario

Sin dall'inizio dell'epoca dell'esplorazione spaziale, quando iniziò a essere prioritaria la necessità di riportare umani e veicoli sulla Terra, crebbero di interesse gli studi sulla fase di rientro, le relative orbite e procedure. Di pari passo, parve chiaro quanto la stabilità influisse sulla buona riuscita del rientro in atmosfera, soprattutto per quanto riguarda la sua accezione dinamica. Ciò presenta tuttora molte difficoltà nella sua formulazione matematica, nella valutazione e nel calcolo, dati i numerosi approcci presenti in letteratura e le numerose definizioni per le derivate di smorzamento aerodinamico.

Lo scopo di questa tesi è quello di identificare un modello affidabile per poter ottenere dati realistici sulla stabilità in rientro della capsula in termini di coefficienti di momento in beccheggio statici e dinamici.

Innanzitutto, è stata scelta una capsula su cui effettuare le successive analisi (Hayabusa) e sono state stabilite le condizioni ambiente del flusso: termodinamica e aerodinamica sono fortemente dipendenti dall'altitudine e dalle variabili di stato, quindi per comprendere meglio la fenomenologia è necessario approntare un set di condizioni univoco, che verrà poi fissato come iniziali e/o al contorno. La casistica scelta prevede un flusso subsonico, che è abbastanza semplificativo visto che non prevede procedure di shock fitting che altrimenti sarebbero necessarie. Tra le altre ipotesi, la geometria della capsula è assialsimmetrica e il moto considerato è solamente sul piano di simmetria del corpo stesso.

Sono quindi state effettuate le analisi con l'ausilio del pacchetto Numeca (composto da un *solutore FINE/TurboTM* e un *grigliatore IGGTM*), approntando diverse analisi per diversi angoli di attacco iniziali, sia per i casi statici sia per quelli dinamici. In questi ultimi, viene impiegata la tecnica delle oscillazioni forzate per poter ottenere quanto ricercato: viene applicato un moto sinusoidale in angolo di beccheggio ai bordi solidi del dominio, mentre forze e momento sono parallelamente monitorati per poter permettere di estrarre i coefficienti di stabilità. Ciò è stato fatto tramite un codice Matlab, che confronta anche due degli approcci disponibili e presenti in letteratura.

Questi risultati sono quindi comparati a un database disponibile in letteratura e basato sugli esperimenti di Hiraki et al.; quindi sono tratte le opportune

conclusioni.

Dato che le ipotesi fatte e le condizioni operative sono state restrittive e semplicistiche, vengono quindi esposte le limitazioni e i possibili sviluppi di questa tesi: lo scopo del progetto non era di ottenere risultati precisi, ma invece di trovare un metodo funzionante e manipolabile per poter condurre analisi ricavandone dati affidabili.

Acknowledgements

First of all, I would like to acknowledge my supervisors, Prof. Domenic D'Ambrosio, Cosimo Chiarelli and Vincenzo Mareschi: their daily support and availability towards me have been determinant and truly appreciated during every peculiar moment and they also gave me the opportunity to pursue my interests with this interesting thesis project. I would gladly thank the people present in the Aerothermodynamic, Mission Analysis and Propulsion Unit, for making me feel as part of the team, and for welcoming me every single morning: their help, words and smiles meant a lot.

Thanks also go to the people that shared with me every break time during these months: the Cactus group and particularly Marta, who guided me through the very first steps inside Thales, and is still a dear friend, but also Ambra, Chiara, Enzo, Gianni, Giorgio, Lucia, Mariano, with whom I exchanged advices, but also enjoyable everyday life bits.

The next acknowledgement goes to my family: Giorgio, Adriana, Alice and her husband Nicolò, for their precious and continuous support, without which I would have never made this path as peacefully as I actually did, despite the common anxieties. Their hand was always there to help me and giving me strength, never wanting something in return if not pure love. Thank you, even just for being there. Special thanks go also to my wonderful grandparents, the ones present and the ones that cannot be: your presence was constant, still, and your prayers were a fundamental help to my succeeding.

As part of my special family, one of the people I am most thankful to is my boyfriend Vincenzo, dass jeden Tag mir helfen hat: die taegliche Morgen-Berufungen, die kleine Reisen in der Schweiz, die Amatriciana-Nudeln und die einfache geteilte Momente auch haben meine Tage beruhigt. Danke an die kleine weisse Seehunde auch!

I would also like to acknowledge the people that accompanied me in this hard path inside Politecnico: AESA Torino members, both past and present, and the

people I had the chance to know because of them; Laura, Simona, Maria, Peppe, Simone, Paolo, Francesca, Lucrezia, Chiara, friends from the first year, and the duo that shared the path further with me, Daniele and Oscar; the friends from the last year of Aerogas dynamics specialization.

A special thankful thought goes to my historic house-mate Federica, and to my old college mates, Chiara and Claudia: sharing every day with you was an unmissable experience.

These people have made me who I am, and I couldn't be more happy and proud of the person I became. From the bottom of my heart, thank you.

Contents

Summary	V
Sommario	VII
Acknowledgements	IX
List of Tables	XV
List of Figures	XVII
Acronyms	XXI
Nomenclature	XXIII
1 Introduction	1
1.1 Thesis organization	3
1.2 Hayabusa sample return capsule	4
2 Atmospheric re-entry	7
2.1 Atmosphere model	8
2.2 Hayabusa re-entry scenario	10
2.3 The problem of instability	13
3 Analysis Subject Definition	15
3.1 Basic Assumptions	16
3.2 Capsule and domain design	18
3.2.1 Hayabusa CAD model	18
3.2.2 Grid generation with IGG^{TM}	19
3.3 Analyses at different angles of attack	25
3.3.1 Validation Database	25
3.4 Numerical Set-Up	26
3.4.1 Turbulence model	28

4	Stability Computations	31
4.1	Static Stability	33
4.1.1	Static analyses	34
4.2	Dynamic Stability	41
4.2.1	Forced Oscillation Technique	41
4.2.2	Dynamic Analyses	46
5	Validating the model: limitations and future works	57
6	Conclusions	61
	Appendices	63
A	MATLAB Script	65
	Bibliography	73

List of Tables

2.1	Subsonic trajectory approximate points, in bold the ones chosen for further analyses	13
2.2	State variables for chosen point of descent of Hayabusa	13
3.1	Mach and Reynolds numbers	17
3.2	Convergence study on different grids, 2000 steady iterations for each computation, Baldwin Lomax TM.	23
3.3	Speed values - boundary conditions for different angles of attack . .	25
3.4	Turbulence Model study	28
4.1	Static Analyses Numerical Setting.	34
4.2	Computed and database values of static pitching moment coefficient at different angles, and, in the bottom row, the rate $C_{m\alpha}$	34
4.3	Numerical setup for dynamic analyses	46

List of Figures

1.1	Sample return missions architecture (Mars) [NASA]	2
1.2	Hayabusa sample return capsule in Hayabusa2 mission [<i>Le Monde, December 2014</i>].	5
1.3	Hayabusa sample return capsule configuration. [2]	5
2.1	Temperature trend with altitude in US Standard Atmosphere [4] . .	9
2.2	Speed of sound trend with altitude in US Standard Atmosphere [4]	9
2.3	Density trend with altitude in US Standard Atmosphere [4]	10
2.4	Informations retrievable from Hayabusa fetched samples [2].	11
2.5	Outline of Hayabusa path back to Earth [2]	11
2.6	Hayabusa descent in terms of speed and altitude varying with time from entry [10]	12
2.7	Hayabusa descent in terms of dynamic pressure and flight path angle varying with time from entry [10]	13
3.1	Reference system for Hayabusa Capsule. [37]	16
3.2	Flow pattern around circular cylinder. [13]	17
3.3	Hayabusa capsule CAD model.	18
3.4	Hayabusa capsule grid - Butterfly shaped grid detail.	21
3.5	Hayabusa capsule grid - Standalone grid detail.	21
3.6	Total grid view.	22
3.7	Laplace Smoothing basic working principle. [22]	24
3.8	Hayabusa capsule axial and normal forces coefficients at different angles of attack, varying with Mach number [24].	26
3.9	Hayabusa capsule pitch moment coefficient and dynamic damping coefficient at different angles of attack, varying with Mach number [24].	26
3.10	Hayabusa simulation at 10° of angle of attack - Spalart - Allmaras model.	30
3.11	Hayabusa simulation at 10° of angle of attack - Baldwin - Lomax model.	30

4.1	Pitching moment coefficients at fixed angles of attack.	35
4.2	Static derivative values over the angles of attack range analysed. . .	35
4.3	Capsule at $\alpha = 0^\circ$ - Flow visualisation (BL turbulence model). . .	36
4.4	Capsule at $\alpha = 5^\circ$ - Flow visualisation (BL turbulence model). . .	36
4.5	Capsule at $\alpha = 10^\circ$ - Flow visualisation (BL turbulence model). . .	37
4.6	Capsule at $\alpha = 20^\circ$ - Flow visualisation (BL turbulence model). . .	37
4.7	Capsule at $\alpha = 30^\circ$ - Flow visualisation (BL turbulence model). . .	38
4.8	Normal force coefficients at different angles of attack.	39
4.9	Axial force coefficients at different angles of attack.	39
4.10	Errors in % for axial, normal forces and pitching moment coefficients, at various angles of attack.	40
4.11	Identification of oscillations in reference system [32].	42
4.12	Typical experimental setting for oscillating body analyses (<i>Langley stability tunnel</i>) [32].	43
4.13	Body response to forced sinusoidal oscillation (<i>Orion Crew Module CFD simulation</i>) [19].	44
4.14	Example of body response to forced sinusoidal oscillation: C_m versus α of attack [35].	45
4.15	Oscillation at $\alpha_0 = 0$: time step at 3/4 of a complete cycle.	47
4.16	Detail of the same time step as Fig.4.15: grid is deformed as the body oscillates.	48
4.17	Fourier harmonics corresponding to pitching moment oscillation ($\alpha_0=0^\circ, \theta = 1^\circ$).	49
4.18	Fourier harmonics corresponding to pitching moment oscillation ($\alpha_0=5^\circ, \theta = 1^\circ$).	49
4.19	Fourier harmonics corresponding to pitching moment oscillation ($\alpha_0=10^\circ, \theta = 1^\circ$).	50
4.20	Fourier harmonics corresponding to pitching moment oscillation ($\alpha_0=20^\circ, \theta = 1^\circ$).	50
4.21	Fourier harmonics corresponding to pitching moment oscillation ($\alpha_0=30^\circ, \theta = 1^\circ$).	51
4.22	Forced sinusoidal oscillation signal input.	51
4.23	Pitching moment coefficient vs Pitching angle ($\alpha_0=0^\circ, \theta = 1^\circ$). . .	52
4.24	Pitching moment coefficient vs Pitching angle ($\alpha_0=5^\circ, \theta = 1^\circ$). . .	53
4.25	Pitching moment coefficient vs Pitching angle ($\alpha_0=10^\circ, \theta = 1^\circ$). . .	53
4.26	Pitching moment coefficient vs Pitching angle ($\alpha_0=20^\circ, \theta = 1^\circ$). . .	54
4.27	Pitching moment coefficient vs Pitching angle ($\alpha_0=30^\circ, \theta = 1^\circ$). . .	54

4.28 Dynamic damping derivative: values computed (Fourier serie and Angular Speed methods) and from available database. Over the green line the capsule has UNSTABLE behaviour, otherwise it is STABLE.	55
---	----

Acronyms

TASI	Thales Alenia Space Italia
ESA	European Space Agency
NASA	National Aeronautics and Space Administration
JAXA	Japan Aerospace eXploration Agency
LEO	Low Earth Orbit
TPS	Thermal Protection System
DSMC	Direct Simulation Monte Carlo
COESA	Committee on Extension to Standard Atmosphere
RANS	Reynolds-Averaged Navier-Stokes (equations)
URANS	Unsteady RANS (equations)
CFD	Computational Fluid Dynamics
FINE	Flow INtegrated Environment
IGG	Interactive multi-block structured Grid Generator
CFV	Computational Flow Visualization
IGS/IGES	Initial Graphics Exchange Specification
CFL	Courant-Friedrichs-Lewy number
BL	Baldwin Lomax turbulence model
SA	Spallart Allmaras turbulence model
TM	Turbulence Model
NS	Navier Stokes
DOF	Degree of Freedom
PM	Pitching Moment

Nomenclature

S	Reference surface ($D\frac{D}{2}$)	$[m^2]$
ρ	Air density	$[kg/m^3]$
V	Flow velocity	$[m/s]$
p	Pressure	$[Pa]$
T	Temperature	$[K]$
R	Gas constant	$[J / kg K]$
γ	Adiabatic coefficient	
c	Sound speed	$[m/s^2]$
μ	Dynamic viscosity	$[Pa s]$
ν	Kinematic viscosity (μ/ρ)	$[m^2/s]$
Re	Reynolds number ($\rho V R/\mu$)	
M	Mach number (V/a)	
D	Capsule diameter	$[m]$
y	Distance from wall	$[m]$
y^+	Dimensionless wall distance	
h	Altitude	$[km]$
g_E	Gravitational acceleration	$[m/s^2]$
λ_i	Lapse rate dT/dh	$[K/km]$
C_A	Axial force coefficient	
C_m	Pitching moment coefficient	
C_N	Normal force coefficient	
A	Axial force	$[N]$
M	Pitching moment	$[N m]$
N	Normal force	$[N]$
$C_{m+/-}$	Dynamic PM coefficient (angular speed)	

Nomenclature

τ	Stress	[Pa]
τ_w	Wall shear stress	[Pa]
q	Heat flux	[W/m]
k	Thermal conductivity	[W/mK]
Pr	Prandtl number ($\mu c_p/k$)	
δ_{ij}	Dirac delta	
δ	Boundary layer thickness	[m]
u_τ	Friction velocity	[m/s]
μ_t	Turbulent eddy viscosity	[Pa s]
t	Time	[s]
\bar{u}_i	Perturbation (Reynolds decomposition)	[m/s]
\bar{U}_i	Time-average (Reynolds decomposition)	[m/s]
E	Energy	[J]
α	Angle of attack	[° or rad]
θ	Pitch angle	[° or rad]
ϕ	Phase angle	[° or rad]
ω	Pulsation or angular velocity	[rad/s]
f	Frequency	[Hz]
C_{stat}	Static pitching moment coefficient	
C_{sin}	In phase pitching moment coefficient	
C_{cos}	Out of phase pitching moment coefficient	
k	Reduced frequency ($\omega l/V$)	[rad/s]
q	Pitching angular speed	[rad/s]
\dot{q}	Pitching angular acceleration	[rad/s ²]
$\dot{\alpha}$	Angle of attack rate	[rad/s]

Nomenclature

C_{m0}	Mean aerodynamic moment coeff.	
C_{mq}	PM coeff. (pitching angular speed)	
$C_{m\dot{q}}$	PM coeff. (pitching angular acceleration)	
$C_{m\dot{\alpha}}$	PM coeff. (angle of attack rate of change)	
$C_{m\alpha}$	Static PM coeff.	[<i>undef</i>]
A	Oscillation amplitude	[° or rad]
α_0	Initial angle of attack	[° or rad]

Chapter 1

Introduction

Along with the beginning of the space exploration era, came the need to further study other Solar System bodies' composition: the first missions to the moon contributed to the development of *sample return* missions' concept, when Apollo 11 successfully returned approximately 22 kilograms of Lunar surface material in July 1969.

The primary goal is collecting and returning safely tangible samples - even molecules or atoms - from an extraterrestrial location to Earth for being analysed. This trend goes against previous methods that involved the simple collection of pieces of meteorites fallen through the atmosphere to Earth' surface, which proved to be limiting in terms of quality and type of samples. Up to now, humanity has managed to collect samples from six identified Solar System bodies, as well as samples of the solar wind, and gained important informations, that could not be obtained otherwise: despite the availability of instruments capable of remote sensing and advanced telescopes, scientific tools on Earth make *sample return missions* worth the choice and cost.

Among the successful ones, it is worth mentioning: Stardust spacecraft, which returned comet samples and also seven particles of interstellar dust, Hayabusa probe, which returned asteroid samples after a rendezvous, and similarly OSIRIS-REx, whose return from asteroid 101955 Benu is planned for 2023 [11].

In the immediate future, many missions are focused on fetching Mars' surface samples, something that has been already tried, without success, with Mars Climate Orbiter and Mars Polar Lander, while Russia is also working on Luna-Grunt mission to return samples for the Moon, and China from Ceres.

What is of primary importance in sample return missions, is the capability of the probe to fetch safely the sample without damaging or altering its composition to Earth. In recent years there has been increasing interest in small space platforms such as micro-nano satellites/probes, also for matters concerning atmosphere and environment protection and homeland security. In fact, reducing size and mass

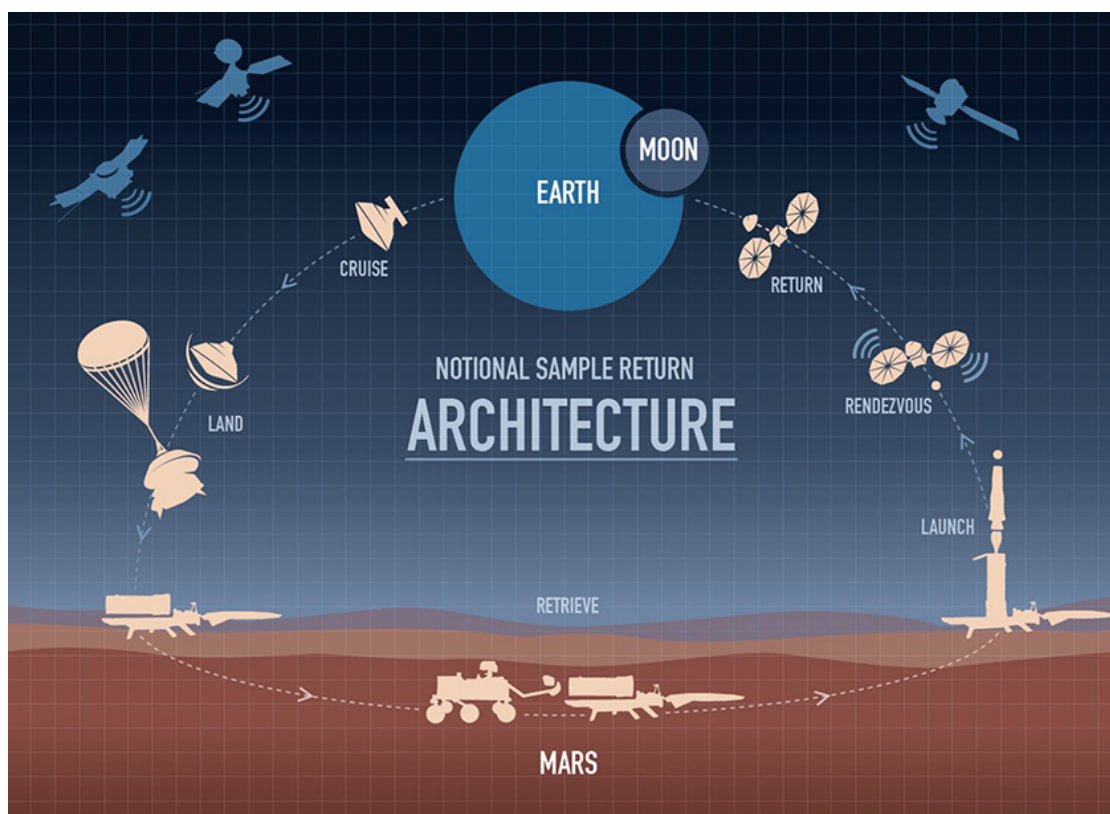


Figure 1.1. Sample return missions architecture (Mars) [NASA]

implies a significant reduction in terms of cost and complexity, which makes these missions more accessible and repeatable.

Despite the pros, there are cons: space debris is a problem aerospace industries are facing, and, since the scientific relevance of a single probe makes it unbearable to be lost, longitudinal static and dynamic stability must be investigated, but this is a question that still has no univoque answer. The purpose in this thesis is, in fact, to develop an efficient method that could fit best the data available on a particular mission of choice: JAXA's *Hayabusa*, previously named as MUSES-C.

This topic has been studied since the 1950s, when space exploration was just taking shape. Due to the drastically different operational environments and geometries of atmospheric entry vehicles, it took years of experimental and analytical practise to develop and acquire an insight into the problem: the analytical work of Allen and Tobak combined with extensive experimental investigations by Bird, Fletcher and Wolhart, Short and Sommer, and others [6] helped to develop the field of blunt-body dynamic stability. An important contribution came from Murman's frequency approach to this issue and later from Teramoto [7], combining analytical

models and CFD flow solver solutions for a study on the Muses-C capsule.

However, different methodologies have been developed ever since and, on the experimental side, three main strategies are used for dynamic investigation purposes:

- Free oscillations technique (easiest experimental setup)
- Forced oscillations technique (easily reproducible on CFD)
- 6DOF-analyses (most difficult and onerous)

where the first two make evidence of the vehicle's response to an input (impulsive or sinusoidal), while the other's aim is to simulate its entire behaviour as well as possible.

These studies show a common result in terms of motion resolution capability, but also underline the unpredictable nature of dynamic stability of these kind of vehicles, as well as the difficulties associated with determining the stability parameters analytically, numerically, and experimentally: the same uncertainties persist nowadays.

1.1 Thesis organization

This work's purpose is to find and validate a valuable method to successfully evaluate stability informations of a blunt body configuration such as a reentry capsule, a model of aerospace purposes' interest.

In the first chapter after this introduction, a brief summary of atmospheric reentry operations and environment is described, along with a deeper analysis on the specific path of Hayabusa, the capsule that will be indeed analysed further. Here, the problem of instability identification and avoidance is underlined, and the main features of the case chosen for the analyses carried out is highlighted.

In the third chapter the setting of the analyses is fully explained: main assumptions are listed, then the process of creation of CAD and grid are briefly discussed, and followed by the numerical setup. Different turbulence models are also taken into account, and it is underlined how and why different angles of attack will be a subject of the computations. To make this work more clear, this chapter has the specific aim to collect every information about the *making-of* of the analyses from A to Z, also in order to be better reproduced or improved.

The fourth chapter's introduction works as a recall to governing equations that will be actually used by the flow solver, and stability is then described, theoretically and numerically, and differentiated in its two acceptations: static and dynamic. For every kind, methodologies and computations are explained, with respective

literature references. In particular, the forced oscillation technique is presented, since it is one of the interesting features of this work, and different models to treat the output of the latter are outlined.

Then, limitations and future works are described, based on what the model has led to: discrepancies in the computations can be further investigated to improve the whole procedure, grid configuration, numerical scheme, and so on.

Conclusions are so extracted, as a summary of what this work has been possible to pursue.

1.2 Hayabusa sample return capsule

Among different shapes studied by ISAS to be eligible for future planetary expeditions and sample return, Hayabusa shape was adopted since MUSES-C mission in 2003, with its first launch towards asteroid 1998SF36: the capsule plays its role in the final phase of re entry, for bringing the sample to Earth. This same capsule was then further employed in Hayabusa-2 mission, launched in December 2014, and expected to return back to Earth in 2020 (Fig.1.2).

Some requisites had been imposed: it had to be small enough to give an inconsistent contribution to the total weight, and yet should have had enough space for the sample itself, and for various hardwares. Also, stuck to the back, there had to be a container for a single stage parachute. Clearly, these traced the guidelines for the overall design of this capsule shown in Fig.1.3, with the proper allocation of components.

Those are the main installed subsystems [3]:

- Heat shields (TPS)
- Instrument box with torus shaped container for the parachute
- Parachute concerning: cross type parachute (soft landing), pyrotechnical pushers, timer for deployment timing
- 242MHz beacon transmitter for localisation (extracted at 10 km of altitude)
- Power supply: Li-(CF)_n primary batteries
- Sample canister for sealing asteroid sample material
- Separation joint (gives translational and rotational speed to capsule)

and are all covered with carbon-phenolic composite to shield from extra-heating.

Since the capsule alone does not have any propulsion system, trajectory has no mean to be changed: therefore, two other contingency cases are considered other

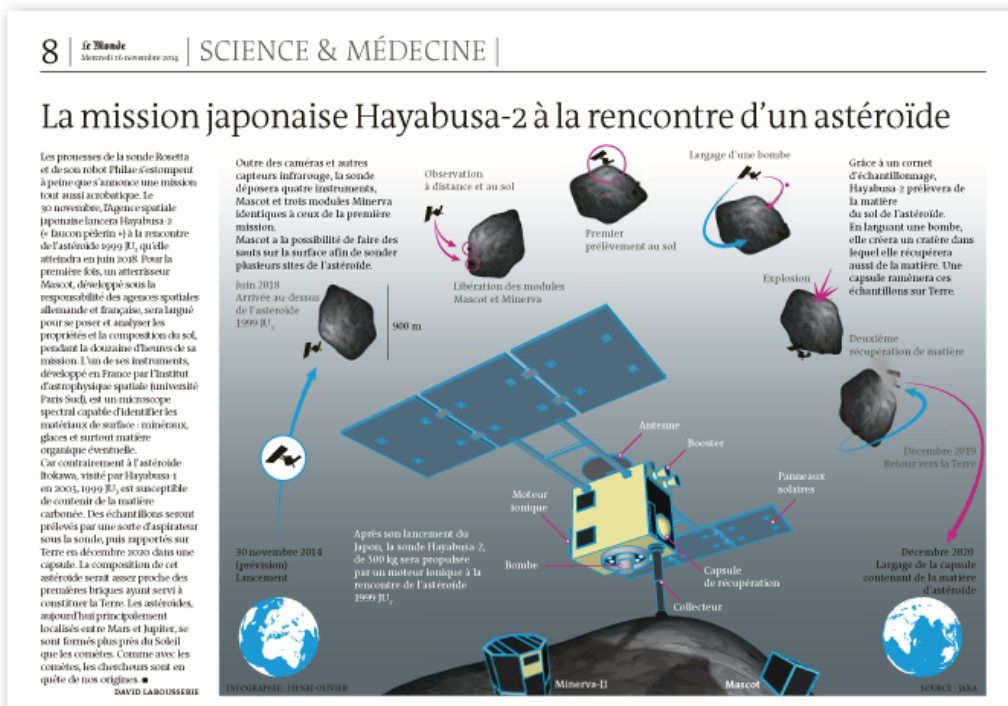


Figure 1.2. Hayabusa sample return capsule in Hayabusa2 mission [Le Monde, December 2014].

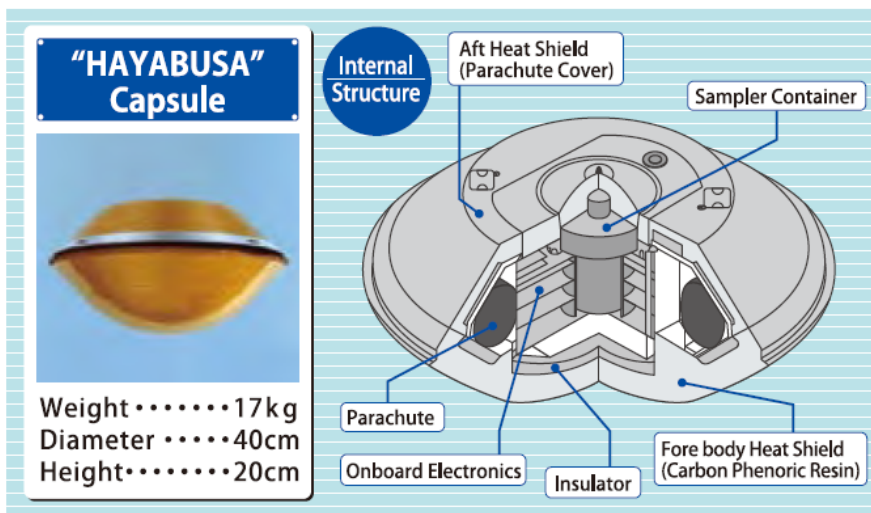


Figure 1.3. Hayabusa sample return capsule configuration. [2]

than the design one. These are established to take into account the worst cases that can occur: in the first, heat shields are not jettisoned and descent is made with no parachute (causing a crash at impact to the ground), in the other one, heat shields are jettisoned, exposing the inside to strong heat fluxes [3].

Another important matter concerning re entry operations is thermal protection: high temperatures can strongly damage the materials of which the capsule is made and the sample itself. That is why the TPS engineer must design the structure with proper materials (ablative, refractory) so that absorption/emission/management of heat loads are well handled. Those aspects, anyway, will not be considered in this work.

Chapter 2

Atmospheric re-entry

There are different types of re-entry procedures [9], based on which forces are acting on the vehicle:

- Ballistic, where the only force acting is the one in the same direction as the motion and its action is retarding (drag contribution). This is typical for re-entry vehicles, decoys,.. such as Mercury and Hayabusa capsules.
- Lifting, where the primary force generated is the one perpendicular to the vehicle's path (lift contribution) along with a drag: lift to drag ratio is one of the main design parameters. This can be the case for re entry vehicles that have some manoeuvrability.

The one examined in this work is the first, as the vehicle will be completely "passive" and cannot be actively moved.

So, the capsule only behaves depending on the flow around it, that changes with altitude in terms of chemical composition and thermodynamic variables: there can be identified several bands [1] that will be described below, in which the vehicle should behave as a high-drag device, capable of reducing its entry velocity to sufficiently complete the mission.

At high altitudes, a *free molecular flow* regime can be experienced: here the vehicle interacts with atmospheric gas molecules reflecting or rejecting them through its surface, but these happen to be so rare that can be ignored.

As the vehicle descends further, a *transitional regime* is identified: this band is responsible of the transition between the previous and the next ones. At the lower altitudes belonging to this zone, aerodynamics and heating transfer as we know them start to take place, and, clearly, interaction with molecules can no longer be ignored.

Finally, the capsule enters the *continuum regime* zone: here the flow's behaviour is completely coherent with Navier Stokes description, and covers the range from hypersonic to subsonic conditions.

Clearly, the latter is the most easily reproducible one both analytically or via CFD, because of its structure. The transitional regime flow is often simulated employing the *Direct Simulation Monte Carlo* (DSMC) method, on statistical bases. What's more, engineering approximations are built as a function of the free-stream Knudsen number, that show good agreement with DSMC [1].

2.1 Atmosphere model

Setting analyses and making calculations concerning a vehicle's insertion in orbit of path through atmosphere requires some knowledge of properties and characteristics of the latter.

One may think of atmosphere as a serie of concentric shells surrounding the surface:

1. The first layer, the *troposphere*, covers the range from sea level to about 10km. Together with the tropopause, it constitutes the *lower atmosphere*.
2. The second layer is the *stratosphere*, and here lies the ozone layer. This zone extends to an approximate altitude of 50km.
3. Surrounding the stratopause, there is the third layer: the *mesosphere*, that ends at about 90km above the sea level. The mesopause is a following thin layer that separates the middle atmosphere from the upper one, the *thermosphere*, where solar activity affects chemical and thermodynamic properties of atoms and molecules. There lies the region of LEOs.

Of course, a little variability in local characteristics or state parameters may be present. For engineering and scientific purposes, this may be source of mistakes and can corrupt the repeatability and reliability of tests/analyses. That is why it is helpful to have a standard basis to refer to. Though a variety of models is available and discussed in the *Handbook of Geophysics* (1985), it is common practise to use the U.S. Standard Atmosphere, redacted in 1976 by COESA (Committee on Extension to the Standard Atmosphere) collecting data from experimental results and the perfect gas theory [5].

Gradients of pressure, temperature and density over the atmosphere's extension can be sum up in Fig. 2.2, 2.1, 2.3, where, concerning the lower atmosphere - of our main interest - one may compute the precise values of state variables through these relations [5]:

$$T = T_i + \lambda_i(h - h_i) \tag{2.1}$$

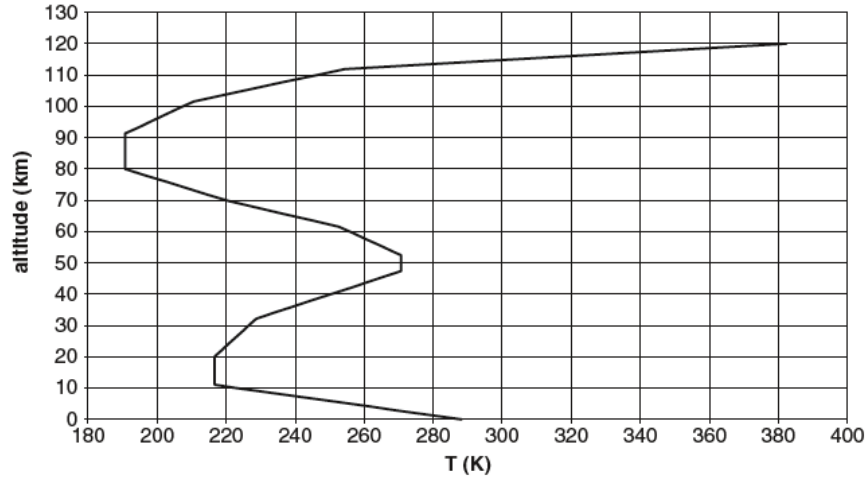


Figure 2.1. Temperature trend with altitude in US Standard Atmosphere [4]

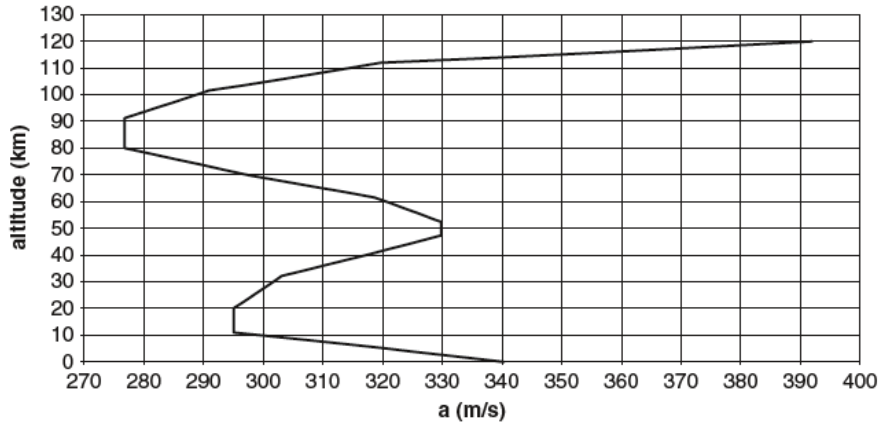


Figure 2.2. Speed of sound trend with altitude in US Standard Atmosphere [4]

$$p = p_i \left[\frac{T_i}{T_i + \lambda_i(h - h_i)} \right]^{\frac{g_E}{R\lambda_i}} \quad (2.2)$$

where T_i and p_i are variables at the start of the layer, λ_i is the lapse rate dT/dh of the corresponding layer, and $g_E/R = 34.17 \text{ K/km}$. From these, density is directly computable. For dynamic viscosity computation, Sutherland's law will be employed.

Gas models must also stick to the relative phenomenology, depending on the Mach number of the free stream flow: as known

- For $M > 1,2$ compressibility effects are not negligible, and a real gas model must be used

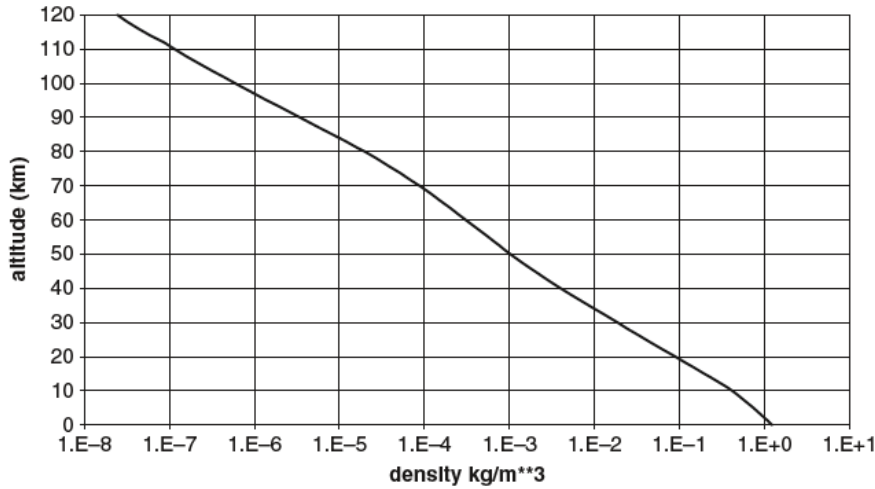


Figure 2.3. Density trend with altitude in US Standard Atmosphere [4]

- For $0.8 < M < 1.2$ transition takes place (*transonic conditions*)
- For $M < 0.8$ subsonic flow follows *perfect gas equation*, at best in a range of Mach below 0.3 where the stream is truly *incompressible*.

In this work, the subsonic condition will be of our concern.

2.2 Hayabusa re-entry scenario

Hayabusa capsule came back to Earth from its first mission on June 13th 2010 over Woomera Prohibited Area in southern Australia returning fragments from the asteroid 1998SF36 "Itokawa", and entering the atmosphere with a speed of 12.04 km/s, making it the second fastest human-made object to do so.

The importance of the mission was particularly high because of the information that could have been acquired from the samples: the surface composition of Itokawa, its history, whether any external substances from other bodies ever touched it, and, last but not least, data from solar wind and cosmic radiation [2] (Fig. 2.4).

An important part of the mission consisted in the re entry phase observation - since the capsule did not have any instrumentation in the heatshield - to gain as much data as possible. Though, as post flight analyses showed [8], there were some discrepancies between planned and real trajectory and times. However, an outline of its descent process can be drawn in terms of altitude, speed and time.

First, in the vicinity of Earth, the capsule is deployed from the spacecraft and enters the atmosphere with an approximate speed of 11.7 km/s and an entry

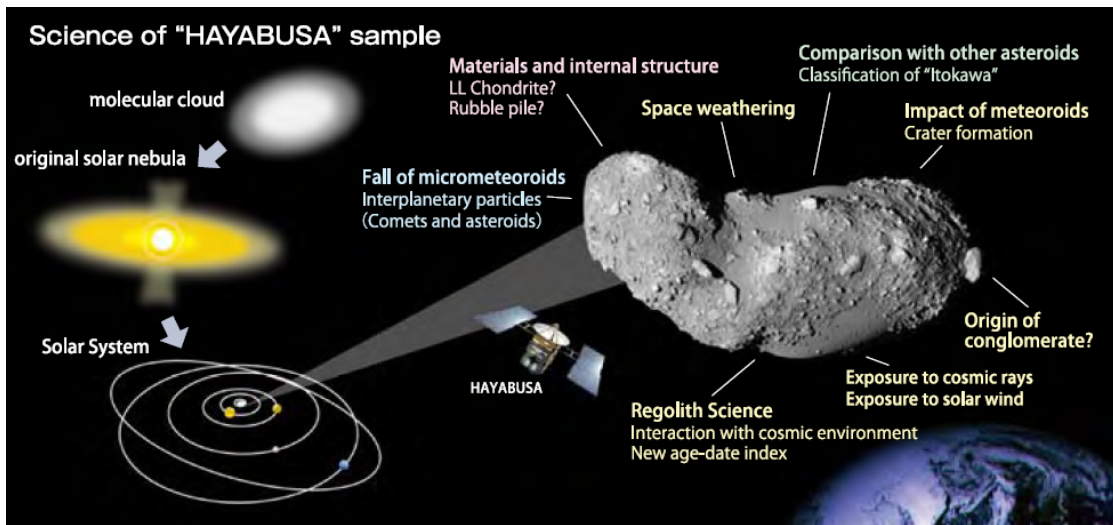


Figure 2.4. Informations retrievable from Hayabusa fetched samples [2].

flight path angle based on the trajectory on design. Then, the aerothermodynamic environment becomes severe for the strong heat fluxes experienced (maximum at 55 km, 60s after re entry), followed by a peak in dynamic pressure (40 km, 70s after re entry). After approximately 227s from re entry, parachute is deployed, contributing to a strong deceleration before landing and next recovery.

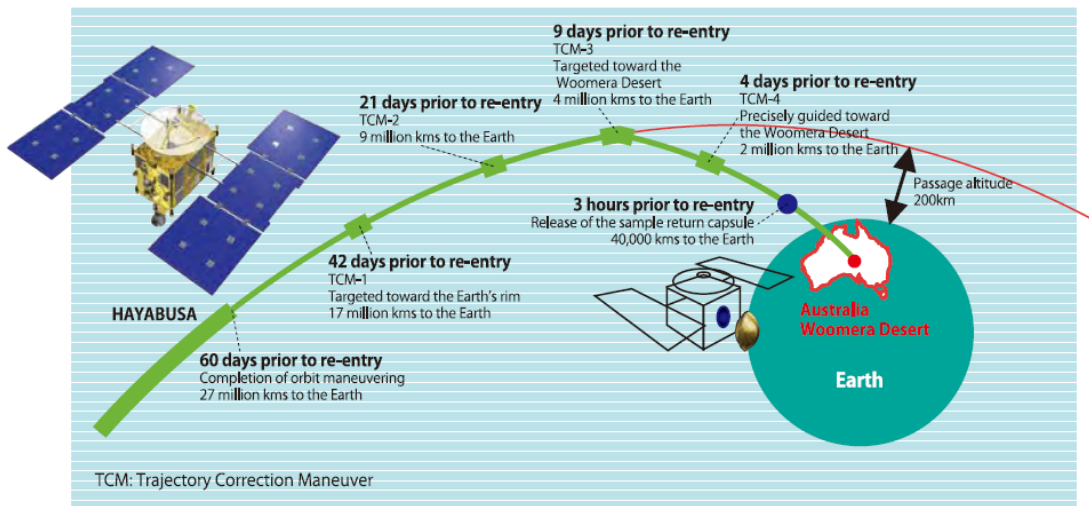


Figure 2.5. Outline of Hayabusa path back to Earth [2]

In more rigorous terms, here is the re-entry and recovery scenario prospected on design:

1. Final trajectory correction manoeuvre for entry targeting: here are a collection of actions aimed to correctly orient the capsule before its deployment. About 9 hours before separation, the capsule is given a Go/NoGo decision for deployment.
2. Ground operation for setting the capsule entry conditions: the capsule is powered on, and power switches from external to internal battery. Then, 8 hours later, release occurs, while the spacecraft undergoes a divert manoeuvre to prevent its reentry.
3. Atmospheric entry: here, the capsule experiences maximum values of heat flux, dynamic pressure, and deceleration (from beginning to 40km altitude).
4. Parachute deploy and descent, with following beacon activation. Here speed decreases to 6 m/s with altitude.
5. Landing and recovery operations take place.

In the last kilometers, though, the capsule sees a change in external flow regime, from hypersonic to subsonic (22km): in this work, it will be analysed Hayabusa's behaviour in subsonic regime, with no coupling effects coming from aerothermodynamics, which strongly affects supersonic and hypersonic regimes.

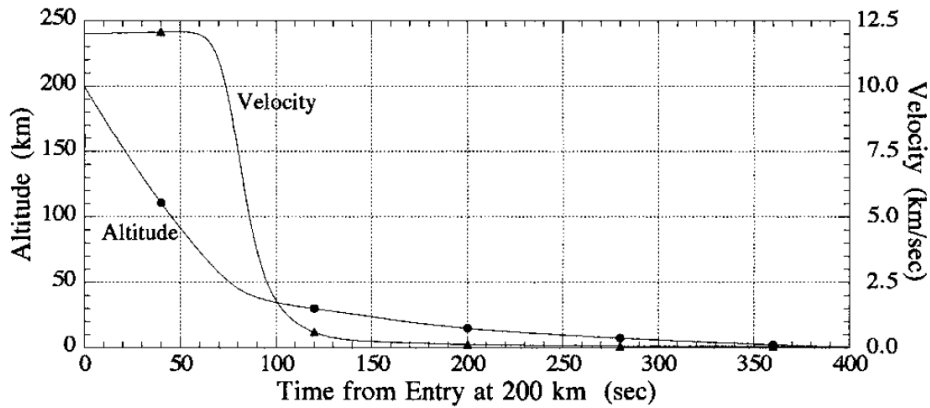


Figure 2.6. Hayabusa descent in terms of speed and altitude varying with time from entry [10]

From Fig.2.6, it is possible to extrapolate enough data to identify a good point for our simulations (Tab.2.2), then, recalling state variables relations, one can get environmental data of the external flow easily (Tab.2.2).

These data will be recalled in the analysis setup, for they will be the boundary condition imposed on the stream.

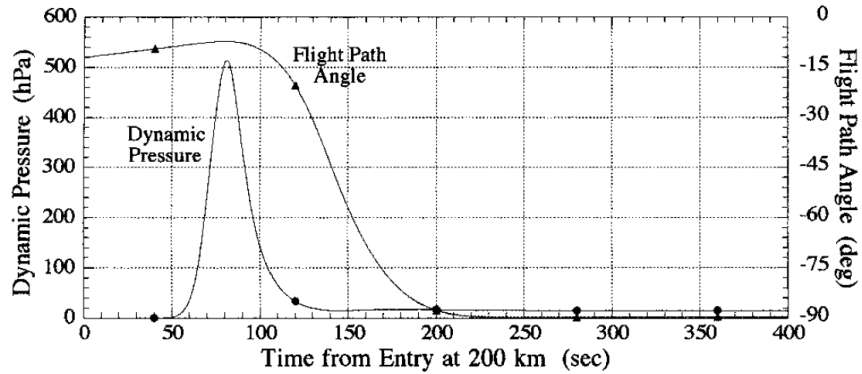


Figure 2.7. Hayabusa descent in terms of dynamic pressure and flight path angle varying with time from entry [10]

Speed (m/s)	Altitude (km)	c (m/s)	Mach
282,06	21,98	295,1	0,955
161,76	19,59	295,1	0,548
169,43	14,73	295,1	0,574
112,44	12,33	295,1	0,381
62,66	9,64	336,4	0,186

Table 2.1. Subsonic trajectory approximate points, in bold the ones chosen for further analyses

Atmosphere Data

p (Pa)	19212,6
T (K)	220
ρ (kg/m ³)	0,31871
μ (Ns/m ²)	1,4E-05

Table 2.2. State variables for chosen point of descent of Hayabusa

2.3 The problem of instability

As times unfold, the needs to bring a sample or to return a vehicle safely so it could be reused have led to the awareness that reentry stability was indeed a topic to be investigated.

As will be better discussed, the aerodynamic stability of a blunt body with large angles amplitude varies across the speed regimes.

Intuitively, one may think of stability as a matter of trends: the more the speed, the more the body will have the tendency of keeping its path; the less the speed, instead, and the more it will be subdued to disturbances of the external

flow and will experience oscillations that may also diverge leading to a total loss of control. That is why at high-speed regimes (hyper-supersonic) stability is normally assured, and instead the problem enhances in subsonic flows: this leads inevitably to consider every possible influence and choose the best compromise to avoid such a situation.

Through this work, in particular, it will be analysed the capsule behaviour at different angles of attack, keeping geometry and flight conditions fixed.

Chapter 3

Analysis Subject Definition

The purpose of this work is to analyse static and, mostly, dynamic stability of capsules in reentry operations while in subsonic regime.

As for the capsule, the choice was to pick Hayabusa because of some reasons: first, its geometry is simple enough to be easily modeled and to be representative of the general behaviour of a capsule of modern conception. Second, it was the most complete database available, which clearly stands as an advantage in terms of results comparison and reliability.

In the following sections, it will be showed the analyses setting step by step from birth of the CAD model to results' gaining, the assumptions and simplifications.

In this work, *NUMECA* suite will be used both for grid generation and flow solver. *NUMECA* International is a company that develops softwares concerning CFD field of study, and has different suites depending on the customers' needs and application types. The one that will be employed in this thesis is made of three main instruments: a grid generator, a flow solver, and a post processing/viewing tool:

- *IGGTM* is an interactive geometry modeler and a multi-block structured grid generator;
- *FINE/TurboTM* is a CFD flow integrated environment for rotating and non-rotating flow analysis, particularly advised for turbo machinery applications. In this case, it has been chosen for the capability of simulating a forced oscillation motion, that will be of our interest for dynamic stability computations.
- *CFViewTM* is an highly interactive Computational Field Visualisation system, which will be replaced by the use of *TecplotTM* in this work.

First, it is mandatory to establish a univoque reference system. In our case, considering a 0° angle of attack condition:

- X axis is placed as the revolution axis - since this body is one of revolution - in the direction of motion, and is pointed towards the nose of the capsule;
- Z axis defines, along with X axis, a plane of symmetry that splits the body in two halves, and - since it is the axis on which momentum is measured - it is set so that positive momentum values mean an upward motion and vice versa;
- Y axis defines, along with X axis, another plane of symmetry, and is set to complete coherently the reference system.

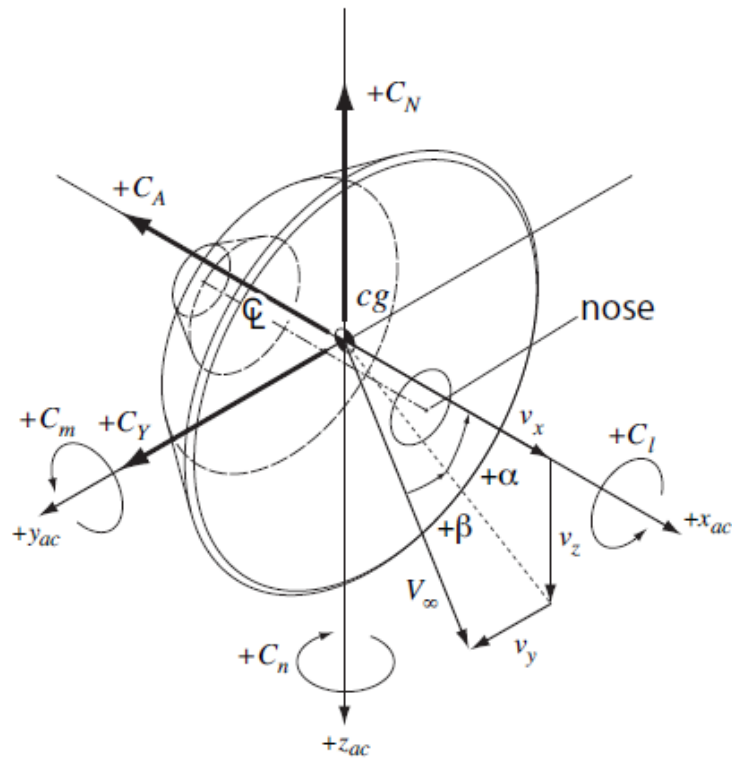


Figure 3.1. Reference system for Hayabusa Capsule. [37]

3.1 Basic Assumptions

Mainly, these are some restrictions to our analyses:

- the center of gravity has a fixed position and locates at 0.12m behind the capsule apex [12], on the X axis; this point's effect on global aerodynamic can be investigated, but it is not of concern in this study;

- the only contemplated motion is the pitching one: stability will be measured at different pitch angles, with no "sideslip";
- analyses will be conducted at different attack angles $[0^\circ, 5^\circ, 10^\circ, 20^\circ, 30^\circ]$, at which both static and dynamic stability will be evaluated;
- from literature [13], it is known how a cylinder's surrounding flow undergoes a change from laminar to turbulent and it is briefly summed up in Fig.3.2.

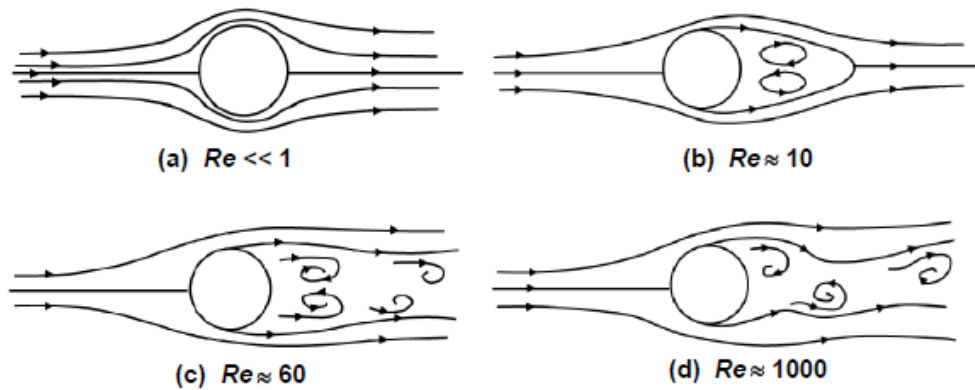


Figure 3.2. Flow pattern around circular cylinder. [13]

Let's suppose there is analogy between Hayabusa geometry and this case: it is realistic to think that the flow will behave in the same way. It then makes sense to state that this is a turbulent case, and a turbulence model must be later selected in the analyses setup;

- the regime is supposed therefore fully subsonic, but not incompressible: perfect gas model is employed;
- the environment, as outlined in the previous chapter, is defined and summed up in Tab. 2.2 with

Mach	0,3795
<hr style="width: 50%; margin: 0 auto;"/>	
Reynolds	991617

Table 3.1. Mach and Reynolds numbers

And these values are supposed constant;

- gravity's effects are neglected;

- defining boundary conditions, solid walls will be assumed as adiabatic.

The modelization that follows will be discussed hereafter.

3.2 Capsule and domain design

Generally, capsule for sample return missions are blunt bodies of revolution. That makes geometry design very easy to be defined. What's more, since the regime analysed in this work is full subsonic, there was not any particular requirement about domain shape (i.e. shock fitting grid, etc.).

3.2.1 Hayabusa CAD model

Hayabusa capsule is very small: it measures 400mm in diameter length, and 200mm in height [7] for a total weight of about 17 kilograms [10]. Its modeling is very simple though, thanks to its structure as a body of revolution.

The capsule used in this work was designed with the aid of DSS *Solidworks* 2015 and successfully exported in IGS format, which can be read by almost every CFD software.

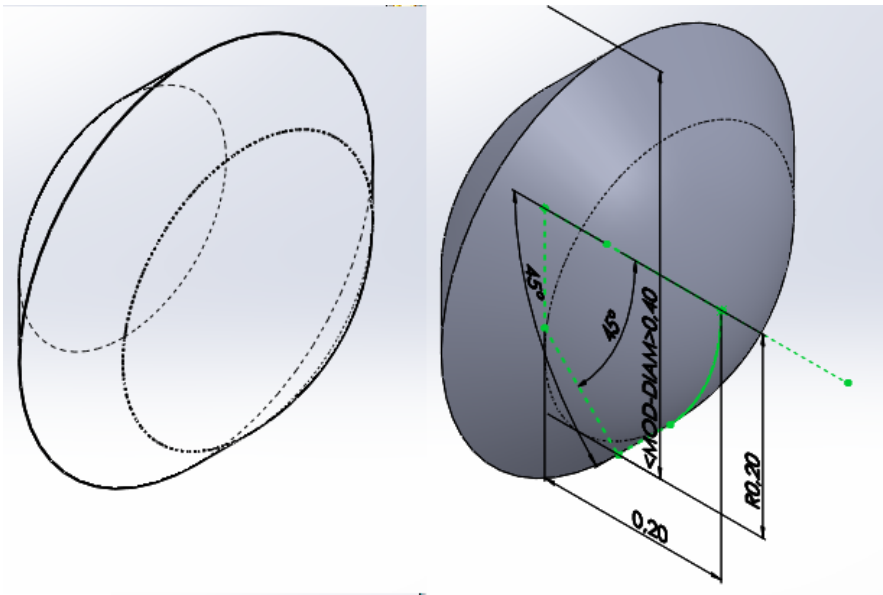


Figure 3.3. Hayabusa capsule CAD model.

An important action to perform is surface creation: bare geometry would have been insufficient in a further process of grid to surface adjustment: that made a CAD modeler's use mandatory.

3.2.2 Grid generation with IGG^{TM}

Grid is a necessary element to compute the flow around the body. For static stability purposes, a fixed grid is sufficient, but is not when it comes to dynamic matters: usually, a *moving grid* approach is preferred, and can be done by rotating the grid along with its solid boundaries [15] or by overlapping two grids (one moving over the other) [16].

However, there are some good practises to apply:

- a 3D grid must be adopted, because of the phenomenology: while airfoil analyses may be led approximating it as a bidimensional body for wings with infinite length, capsule's geometry makes this path impracticable because of the influence that it exerts on the flow;
- structured grids are preferred, which consists in dividing grid structure in more blocks in order to have a better global quality mesh, with proper orthogonality, aspect ratio and expansion ratio [18];
- cells dimension must then stick to phenomenology: grid must be refined where gradients may be strong (i.e. near edges) and must also be appropriate to catch how flow evolves. Attention must also be paid to dimension of adjacent cells, which must not create strong differences that could negatively affect the computation: the transition must be smooth;
- concerning domain dimensions, it is a good practise to have a grid about 10-15 diameters large in every direction compared to the capsule [19]. Plus, no particular architecture is required since no shocks occur;
- grid points must trace perfectly the body' surface in order to have more accurate simulations;
- boundary layer grid elements must be small enough to capture the viscous sublayer. For this matter, one may refer to the adimensional turbulent coordinate y^+ , as follows in Eq. 3.1 [17].

$$y_{wall}|_{(y_+=1)} = 6 \left(\frac{V_{ref}}{\nu} \right)^{-7/8} \left(\frac{L_{ref}}{2} \right)^{1/8} y_+ \quad (3.1)$$

where y_+ is set to 1 (start of viscous sublayer), and can be otherwise defined as in Eq.3.2

$$y_+ = \frac{y u_\tau}{\nu} \quad (3.2)$$

where friction velocity is $u_\tau = \sqrt{\frac{\tau_w}{\rho}}$, dependant from wall shear stress;

- cells number must also concern computational resources: simulations must not be too onerous, nor too approximate, a compromise must be found.

At this point a preface can be clarifying: since at one stage of the analyses a pitching motion will have to be performed via forced oscillations, and since this motion in the software of use can be only applied to solid boundaries (i.e. the capsule itself), it was necessary to think of the best strategy to generate a domain grid that could let to do so using the tools at our disposal.

Grid composition

As said, grid generation was performed with *IGGTM*, part of Numeca suite.

The first step was importing the CAD model in the grid modeler, and domain was then built on its boundaries and surfaces, performing the mesh just on one half of it: this choice was made in order to get a lighter computational cost, and since the phenomenology to be studied takes place symmetrically, it was not unfounded.

What's more, adopting a *cartesian* solution lets identify every node as a combination of three different indexes, along the three directions I, J, K, with each block having a separate, independent reference system of this kind. The overall grid was divided in four different blocks made of exahedral elements with different features based essentially on the body's geometry:

1. The first block extends to 10 times the diameter further of the forebody tip and was set on the nose of the capsule: here the main requirement is to stick to the curved surface, and also to get a grid with no triangular elements, especially near the edges on the symmetry plane. This aim was pursued by setting a *butterfly configuration*, as showed in Fig.3.4 and by modifying properly its parts' edges so that no shape gradients are there.
2. The second block is specular to the first, on the tail of the capsule shape: a butterfly configuration is adopted again for the same reasons, and its extension is enlarged to 15 times the diameter. This time, the surface to stick to is plane, so there were less difficulties concerning mesh projection, but there were some issues imposing a specific cell spacing, and that is why this block was split in its four parts: one *inner block*, and *parent blocks*.
3. The third and fourth block are placed between the first ones, and their division is made to have a better control on edges spacing, ortogonality and surface sticking.

Every of these blocks have been set to "fluid" as type. Concerning distribution, in every block has been set a first cell spacing of 1E-06 meters where the boundary

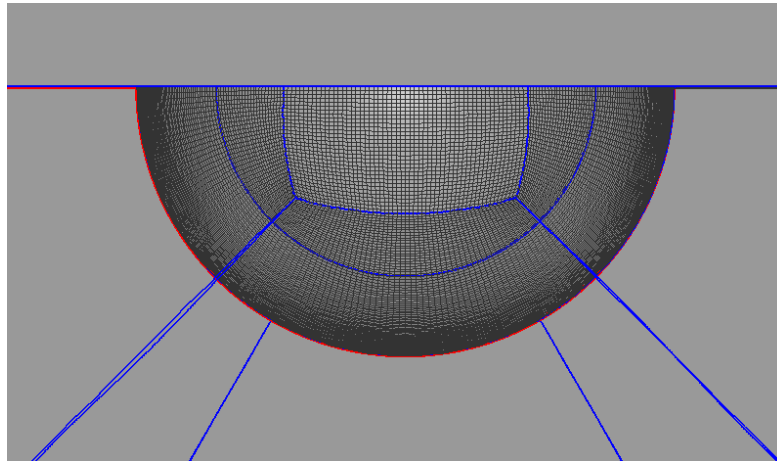


Figure 3.4. Hayabusa capsule grid - Butterfly shaped grid detail.

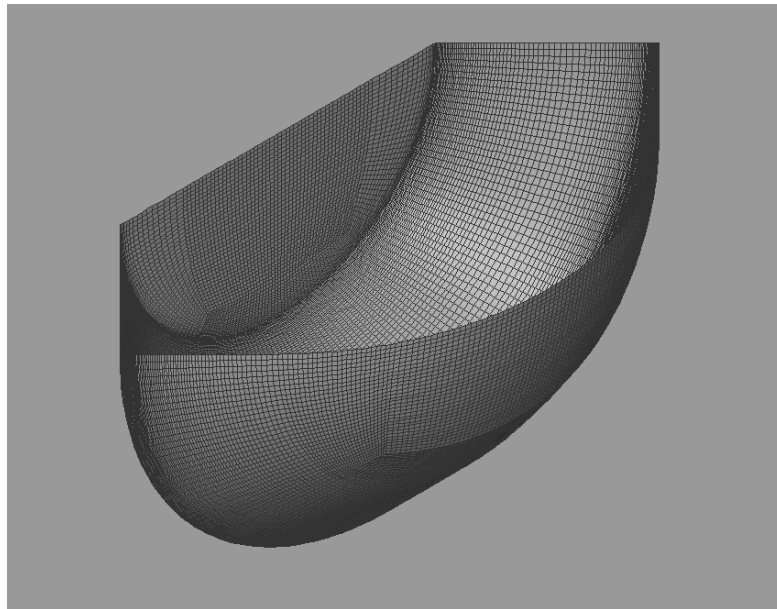


Figure 3.5. Hayabusa capsule grid - Standalone grid detail.

layer lies [19] and a refinement of about $5E-04$ meters where there were sharp edges in the body geometry. These numbers have come from a study regarding two main aims: getting a mesh with good convergence properties, and getting an efficiently working *multigrid structure*.

Multigrid structure is a feature of IGG^{TM} : it corresponds to "the capability of extracting coarser grids several times by skipping over two points in each block direction" [18]. This practise is highly recommended because it ensures convergence

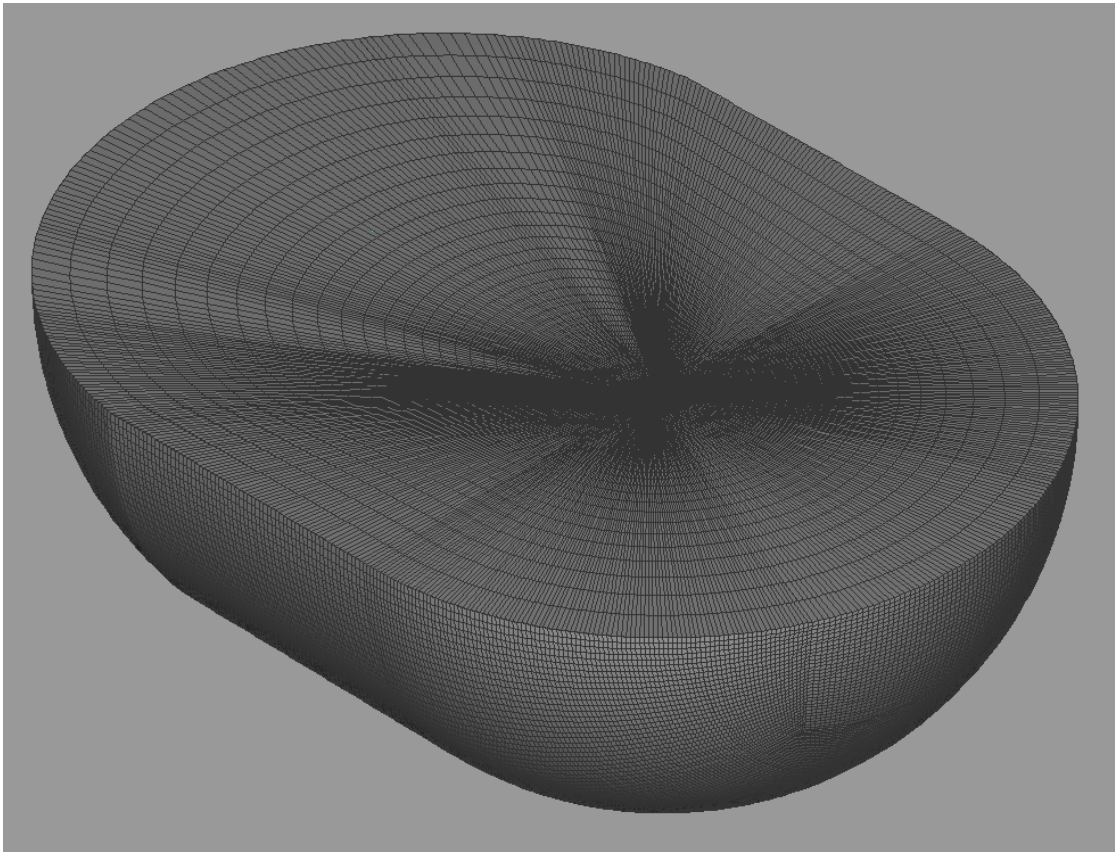


Figure 3.6. Total grid view.

of the flow solver, and that constrains the choice of particular number of points, that must be *<number of levels desired>* times dividable by 2.

A grid convergence study was performed, and it is discussed further in the following section.

Grid convergence study

Convergence study is performed in order to achieve best accuracy at the lower computational cost possible. Convergence is a condition reached when the final solution is identified, usually after a certain number of oscillation cycles; this process can be monitored thanks to *residuals*. In a steady state simulation, when analysing for example a general continuity equation such as Eq. 3.3, where a time dependent term of a generic variable "X" equals a flux term:

$$\frac{\partial X}{\partial t} = \nabla X \quad (3.3)$$

the right-hand term should approach to zero. Since, though, the numerical value will not be precisely that, this is called *residual*. Its rate of decay, when high, is a figure of merit for a solving algorithm [26].

In *FINE/TurboTM* they are computed as the imbalance in the linearised system of discrete equations, that is the sum of the imbalance in each cell (Eq.3.4):

$$RES = \sum R(U) \quad (3.4)$$

then the root mean square of the residual is computed as in Eq. 3.5:

$$RMS_{RES} = \log(RMS(\frac{RES}{cellvolume})) \quad (3.5)$$

and so the maximum of the residuals (Eq. 3.6):

$$MAX_{RES} = \log |MAX(\frac{RES}{cellvolume})| \quad (3.6)$$

with logarithms to the base ten [17].

Different grids were put to the test, with same shape, but increasing number of points. Consulting approaches available in literature, four grids were tested, with total cells number variable with the power of 2: 1, 2, 4 and 8 million cells.

Cells	Solution reached?	Limit Cycle?	Max ΔC_m	Name
1E+06	No	Amplitude: $\approx 2,5$ Nm	0,019462741	<i>coarser</i>
2E+06	\simeq	Amplitude: ≈ 1 Nm	0,007785096	<i>medium2</i>
4E+06	Yes	Amplitude: $\approx 0,4$ Nm	0,003114039	<i>medium4</i>
8E+06	Yes, needs + iter	Amplitude: $\approx 0,4$ Nm	0,003114039	<i>fine</i>

Table 3.2. Convergence study on different grids, 2000 steady iterations for each computation, Baldwin Lomax TM.

Tests were conducted at 10 degrees of angle of attack: this because generally, it can be seen from different works how difference between results of different grids spreads when increasing angle of attack.

As can be seen from Tab.3.2.2, meshes with 1 and 2 million cells show a limit cycle behaviour that is probably due to the poor resolution: the mean value is surely approximating the right solution, but it cannot be identified precisely and oscillations keep occurring. In fact, a limit cycle can be expected from this type of application, since the nature of the phenomena involved is very unsteady due to the recirculation zone behind the capsule, after stream separation [27]. Limiting its amplitude is the best choice to get close to convergent results. That is why,

despite the computational cost in matters of time and resources, the grid chosen for our computations is the one with 4 million cells.

The convergence study practised in this study was addressed to verify convergence in a preliminary stage of analyses: no meshes with number of cells higher than 8 millions were investigated because it would have taken too much computational time to converge to solution, as can be also seen with the latter. Indeed, the final grid was chosen so that there was a good compromise between accuracy and computational time. Unfortunately, the total number of points ($4 * 10^6$) seems to be not enough for precise results when compared to those employed in other studies [14], and could be surely one of the topics to better investigate on in further studies.

Laplacian Smoothing tool

Instead of the mentioned techniques, laplacian smoothing is the method used to treat moving grids in this work. This assumes that the mesh deformation caused by a moving solid boundary is so small that can be approximated just by a smoothing operation, without editing mesh topology nor generating negative cells in the domain [17].

Moving vertices in new positions is an operation that can be pursued in different ways, each one based on a proper theory [22], but the basic idea is to move every node to the geometric centre of its neighbors [23]. More accurate methods provide the chance to constrain mesh cells' points and give them a sort of weight depending on curvature, position, and so on. Then, a mathematical model can iteratively predict their new position, from the starting informations.

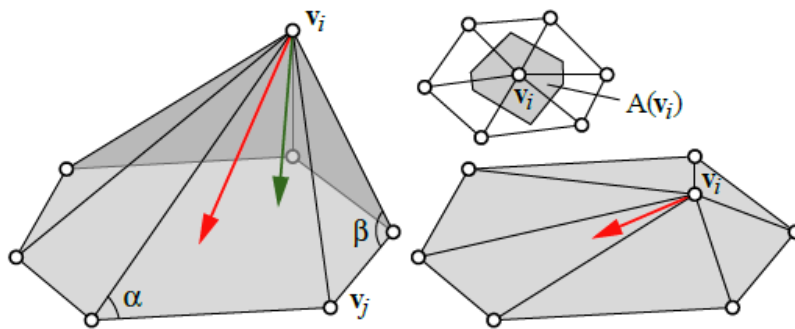


Figure 3.7. Laplace Smoothing basic working principle. [22]

This tool is often used also in computer graphics, because it is computationally inexpensive, can be very adaptable and can be optimised. However, it does have

undesirable properties: it can invert mesh elements and is very sensitive to the order in which nodes are smoothed.

For our case, a feature called "*weighted smoothing of displacements*" was enabled in order to avoid negative volumes, especially for small cells, during the mesh deformation process; plus, a relaxation factor for improving the efficiency of this procedure was imposed.

3.3 Analyses at different angles of attack

In matters of stability, it is important to determine a range/value where the body analyzed is stable (statically or dynamically). That is why, dealing with this topic, different angles of attack have to be studied.

To determine which angles must be investigated, a comparison with the reference database at our disposal was made, highlighting this set: [0°, 5°, 10°, 20°, 30°].

Since it was not possible to vary the capsule's angle, speed vector was split in its *sine* and *cosine* contributions, and was given, along with atmosphere conditions, as *boundary conditions* to every computation (Tab. 3.3). In the case of 0 degrees of incidence, they were also set as initial conditions: for the other cases, those were replaced by the results of the computation at lower angle of attack.

	0°	5°	10°	20°	30°
V_x [m/s]	112	111,574	110,298	105,246	96,995
V_y [m/s]	0	9,761	19,449	38,306	56,000

Table 3.3. Speed values - boundary conditions for different angles of attack

3.3.1 Validation Database

Thanks to M. Sudars [*Thales Alenia Space Italia*], it was possible to get precise values of C_A , C_N , C_m and C_{mq} graphs, already present in literature [7].

As we already mentioned, our analyses take place in subsonic range, at a very low Mach number (0.38), though in compressible flow regime. Below, are summed up graphs and values at those selected conditions that will be used as a validation tool during this work.

Note that this database is made of experimental results coming from *free oscillation tests* [25] at least in subsonic regime - for $M > 4$ simulations were made instead -, which is of this work's interest. Plus, dynamic damping coefficients were

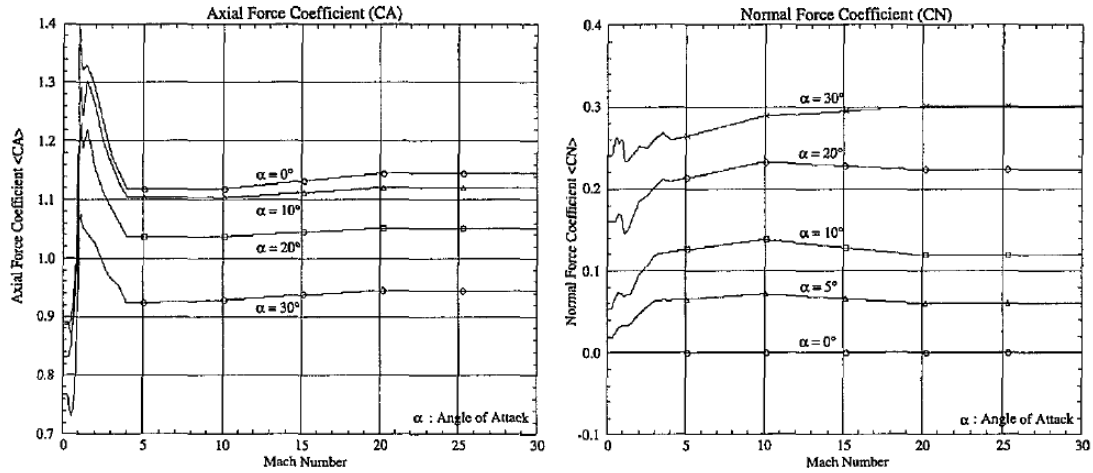


Figure 3.8. Hayabusa capsule axial and normal forces coefficients at different angles of attack, varying with Mach number [24].

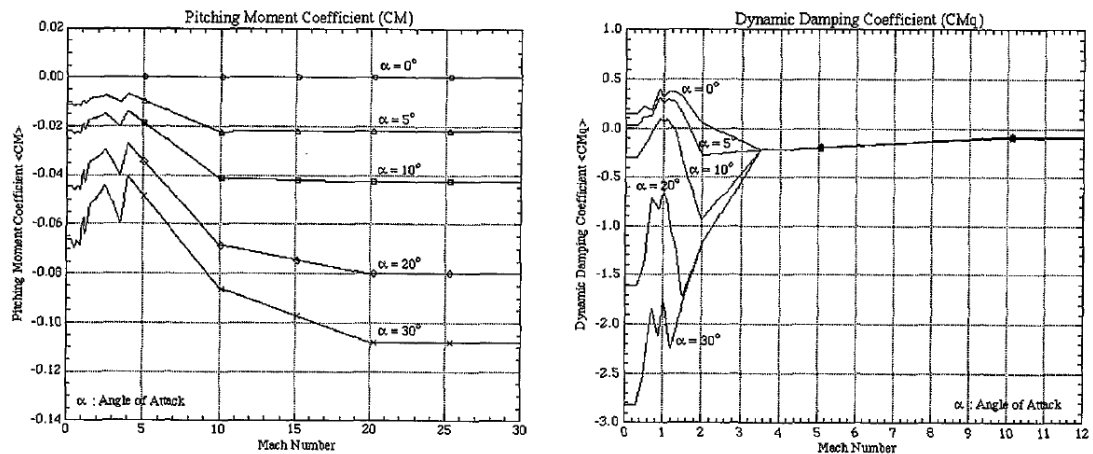


Figure 3.9. Hayabusa capsule pitch moment coefficient and dynamic damping coefficient at different angles of attack, varying with Mach number [24].

extracted via *attitude motion numerical simulations*, that, in this thesis, were unable to be reproduced. In fact, this kind of simulations are usually performed with onerous softwares that compute dynamic laws of motion with 6 DOF.

3.4 Numerical Set-Up

Defining the numerical method to lead an analysis means to select those parameters or models employed by the flow solver when finding the flow solution.

As for parameters, this is what can be chosen.

- CFL number: this is the *Courant-Friedrichs-Lewy* condition, and it proves to be really determining for the computation stability. In time-dependant computations, it can be defined as a condition on the speed with which the flow solver covers a cell, compared to the speed of the flow, and the criteria pronounces that:

$$CFL = |V| \frac{\Delta t}{\Delta x} \leq 1 \quad (3.7)$$

In practise, this criteria is used by flow solvers also in steady simulations, as a tool to improve calculus stability. Indeed, in such cases, it can be even higher than 1, because the possible transitory is not of interest, and increasing this number proves to be good to accelerate the process to convergence.

- Number of multigrid levels: as said before, this tool is specific of the flow solver. Once a grid is done, with its proper number of grid levels depending on the number of points distributed in every block in every direction (I,J,K), one may choose how many of them to employ in the computation. It is recommended to use almost three to get a true benefit from its application.
- Spatial discretisation scheme: usually, for steady computations, a second order scheme like *central differences* is employed. For unsteady computations *upwind* scheme is the most used, and most efficient for this kind of computations: a first order upwind scheme will be then applied to preserve a quite light computational cost.
- Time discretisation scheme: for unsteady computations, *dual time stepping method* proves to be a very useful tool to reach the desired accuracy [28]. It enables the solver to perform some inner iterations (fixed number, or until the convergence criteria is satisfied) to avoid any transitionary effect: at least 10-15 inner iterations are advised. Anyway, the software of use is set up so that
 - The first time step of the unsteady computation is performed with a *first order upwind in time* in time;
 - Every other iteration is performed with a *second order upwind in time* scheme.

In this work, will be displayed the numerical setting chosen for every simulation, time by time.

3.4.1 Turbulence model

Turbulence is a chaotic state of the flow, that occurs at very high Reynolds numbers. Simulating or determining the flow's conditions in such a regime can be only done by models based on a statistical approach (RANS - URANS).

Of course, depending on the type of flow/body there are turbulence models that better adapt to certain situations [20]. The case presented in this work involves a separation at the edge of the front part of the capsule, for shape reasons: this simplifies turbulence computation since the point at which the flow separates is geometrically fixed, and therefore even simple models might be chosen. The most commonly used models for this kind of cases are two: Spalart-Allmaras, a one-equation model, and Baldwin-Lomax, an algebraic one [21].

Those models differ one from another for the definition of the so called "*turbulent viscosity*", a term that comes from the Boussinesq approximation: the Reynolds stress tensor in the time averaged NS equations is replaced by an expression dependent from this turbulent viscosity μ_t [29].

From Boussinesq, one gets the general equation (Eq.3.8):

$$\overline{\rho u_i u_j} = -\mu_t(\overline{U_{i,j}} + \overline{U_{j,i}}) + \frac{2}{3}\delta_{ij}\rho k \quad (3.8)$$

where δ_{ij} is *delta of Dirac*, and u, U are the components of Reynolds decomposition for speed in perturbation and average contributions respectively.

<i>Mesh</i>	Baldwin - Lomax	Spalart - Allmaras		Database
<i>medium4</i>	-1,111538343	-1,083674166	<i>M (Nm)</i>	-0,0366
	-0,034613733	-0,033746032	<i>C_m</i>	
	5,426959368	7,797727694	<i>err %</i>	
	89,91544888	92,76266584	<i>A (N)</i>	0,889765
	0,560000354	0,577733041	<i>C_A</i>	
	37,06199342	35,06903045	<i>err %</i>	
	8,916336658	10,67121347	<i>N (N)</i>	0,055401
	0,055531633	0,066461141	<i>C_N</i>	
	0,235794963	19,96379302	<i>err %</i>	

Table 3.4. Turbulence Model study

While studying grid convergence, a parallel turbulence model evaluation was set up with the final grid, comparing those models, and improving Spalart-Allmaras' one with the extended wall function, that should give better results when coming

to curvature effects of the flow. Since computing times required by BL model were lower, convergence study with steady computations was pursued with the latter: once identified the grid with best convergence properties, a second verification of the turbulence model was done.

As can be seen from Tab. 3.4.1, the SA model seems to be needing an even higher cells number to reach the same accuracy of the BL one: for computing times and more stable convergence, in this work, the second choice was preferred, and since also Teramoto and other experts of the topic employ BL [7], this seems a reasonable choice. In fact, what truly affects stability coefficients, concerning turbulence, is separation, that is well located here.

However, this advantage is paid with lower quality of the flow's resolution in visualizations (Fig.3.10 and Fig.3.11), which will be strongly affecting results at high angles of attack, as will be seen.

In a preliminary stage of simple validation like this work, BL gives very good results without employing a large computing power, keeping the model fast and light, but the user must be aware that, for a good physical representation, at least SA model must be used, increasing the number of iterations and cells necessarily.

Of course, employing a more accurate model ($k-\epsilon$, $k-\omega$, ...) could be a chance to get more precise results, and could be an object for further studies.

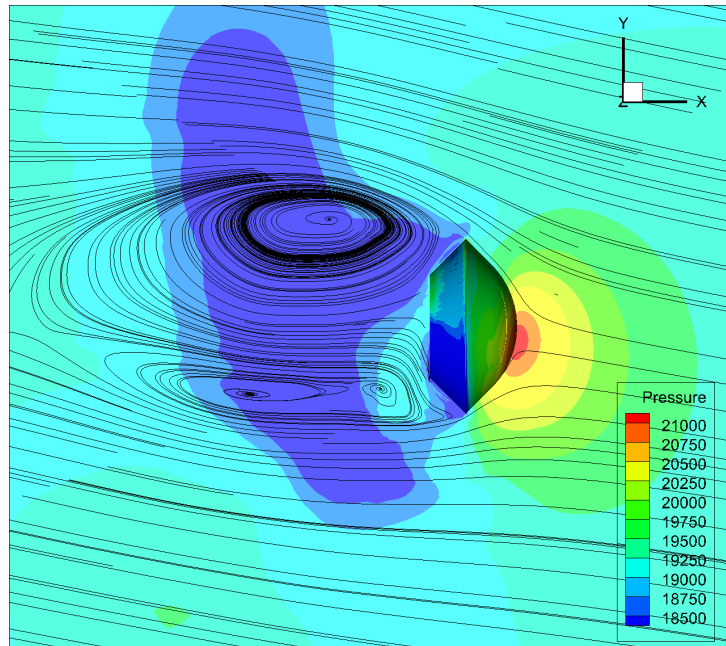


Figure 3.10. Hayabusa simulation at 10° of angle of attack - Spalart - Allmaras model.

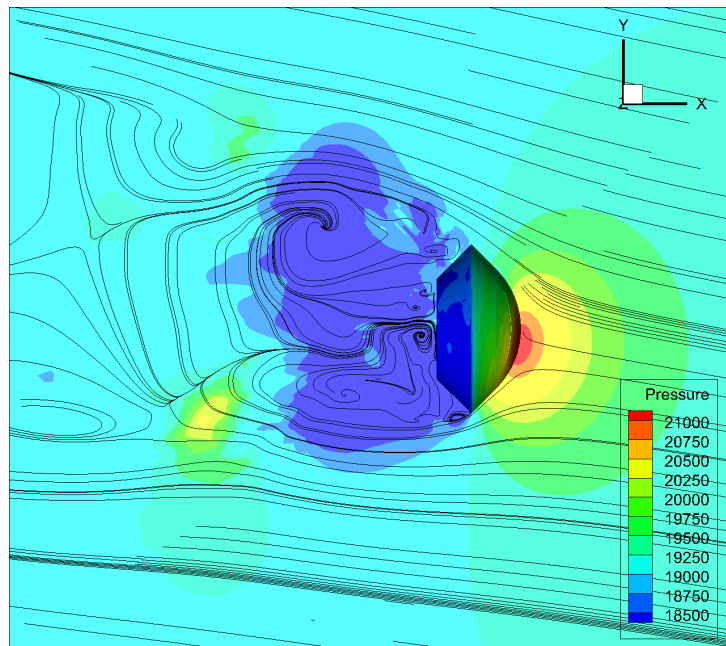


Figure 3.11. Hayabusa simulation at 10° of angle of attack - Baldwin - Lomax model.

Chapter 4

Stability Computations

For the reasons explained and discussed in the previous section, analyses are conducted referring to three-dimensional, compressible, continuous, subsonic flows.

Governing Equations

So, every computation refers to a flow modelization that it described by Navier-Stokes *governing equations*, a non linear partial differential equations' set derived by G.G. Stokes in early XIX century. They present an addition of the term relative to flow viscosity, neglected instead in the older Euler model. Physically, those equations represent conservation time-dependent laws of mass (Eq. 4.1), momentum (Eq. 4.2, 4.3 and 4.4) and energy (Eq. 4.5) along the three directions.

$$\frac{\partial \rho}{\partial t} + \frac{\partial(\rho u)}{\partial x} + \frac{\partial(\rho v)}{\partial y} + \frac{\partial(\rho w)}{\partial z} = 0 \quad (4.1)$$

$$+ \frac{\partial(\rho u)}{\partial t} + \frac{\partial(\rho u^2)}{\partial x} + \frac{\partial(\rho uv)}{\partial y} + \frac{\partial(\rho uw)}{\partial z} = -\frac{\partial p}{\partial x} + \frac{1}{Re} \left[\frac{\partial(\tau_{xx})}{\partial x} + \frac{\partial(\tau_{xy})}{\partial y} + \frac{\partial(\tau_{xz})}{\partial z} \right] \quad (4.2)$$

$$+ \frac{\partial(\rho v)}{\partial t} + \frac{\partial(\rho uv)}{\partial x} + \frac{\partial(\rho v^2)}{\partial y} + \frac{\partial(\rho vw)}{\partial z} = -\frac{\partial p}{\partial y} + \frac{1}{Re} \left[\frac{\partial(\tau_{xy})}{\partial x} + \frac{\partial(\tau_{yy})}{\partial y} + \frac{\partial(\tau_{yz})}{\partial z} \right] \quad (4.3)$$

$$+ \frac{\partial(\rho w)}{\partial t} + \frac{\partial(\rho uw)}{\partial x} + \frac{\partial(\rho vw)}{\partial y} + \frac{\partial(\rho w^2)}{\partial z} = -\frac{\partial p}{\partial z} + \frac{1}{Re} \left[\frac{\partial(\tau_{xz})}{\partial x} + \frac{\partial(\tau_{yz})}{\partial y} + \frac{\partial(\tau_{zz})}{\partial z} \right] \quad (4.4)$$

$$\begin{aligned}
 \frac{\partial E}{\partial t} + \frac{\partial(uE)}{\partial x} + \frac{\partial(vE)}{\partial y} + \frac{\partial(wE)}{\partial z} = & -\frac{\partial(up)}{\partial x} - \frac{\partial(vp)}{\partial y} - \frac{\partial(wp)}{\partial z} + \\
 & -\frac{1}{RePr} \left[\frac{\partial q_x}{\partial x} + \partial q_y \partial y + \partial q_z \partial z \right] + \\
 & + \frac{1}{Re} \left[\frac{\partial}{\partial x} (u\tau_{xx} + v\tau_{xy} + w\tau_{xz}) + \frac{\partial}{\partial y} (u\tau_{xy} + v\tau_{yy} + w\tau_{yz}) + \frac{\partial}{\partial z} (u\tau_{xz} + v\tau_{yz} + w\tau_{zz}) \right]
 \end{aligned} \tag{4.5}$$

The four independent variable are the spatial coordinates (x, y, z) and time, while the dependent ones are six: pressure, density, temperature and the three components of the velocity vector (u, v, w) . The τ variables are components of the stress tensor and each of them is the second derivative of the velocity components.

One may notice that, in these expression, some physical properties appear as adimensionalized by diameter of the capsule, sound speed, and uniform flow density: Reynolds number (Re) is a similarity parameter that is the ratio of the inertia of the flow to the viscous forces in the flow. The heat flux is the q variable, while the Prandtl number (Pr) is another similarity parameter that represent the ratio of the viscous stresses to the thermal ones.

To gain a solution, this set is discretized and solved by the finite difference method on the employed grid system by the flow solver, with proper cell spacing depending on the region to investigate as already discussed.

What the user gets as output, apart from thermodynamic variables, is essentially the set of acting forces: normal, axial and momentum around z-axis, that are the core results from which stability can be then evaluated. Indeed, only longitudinal stability will be investigated, since the only allowable motion is the one on the X-Y symmetry plane.

Hereafter, will be unfold how coefficients are computed and which models are used to do so, both for static and dynamic stability matters. Calculations in support of the computations' results have been made with a MATLAB code appositely written, accessible in Appendix A.

4.1 Static Stability

When a body is statically stable that means that it has the capability to undergo to a flow coming with a certain incidence without generating a positive pitching moment, i.e. without amplifying the phenomenon. In fact, in unstable situations, an angle of attack generates a pitching moment that increases that angle, leading to a loss of control, especially when, as in such configurations as the one employed here, there is no active motion control.

Static stability, as for aircrafts, can be investigated searching for the connection between variation of attack angle and pitching moment. Since, as a result, the value of the pitching moment itself is given from simulations, some simple operations must be done to achieve informations of concern.

First, the adimensional coefficient is extrapolated as in Eq.4.6:

$$C_m = 2 \frac{M}{\frac{1}{2} \rho V_0^2 S \frac{D}{2}} \quad (4.6)$$

where thermodynamic quantities refer to free stream condition, D is the capsule's diameter, $D/2$ is its total length, and the reference surface is supposed as D^2 . Since though the object of the simulations was only one half of the domain, the surface is only $D^2/2$, and a factor of 2 must then be added to obtain the total coefficient.

In fact:

$$C_m = \frac{M}{\frac{1}{2} \rho V_0^2 D \frac{D}{2} \frac{D}{2}} \quad (4.7)$$

When plotting these coefficients, with the corresponding angles of attack, static stability could be evaluated just qualitatively: a negative rate means the capsule will be stable in that range.

Analitically, the rate can be computed as a common derivative of a straight line: this operation was easily conducted with MATLAB, yet using a second-order accuracy scheme with expressions depending on points' position inside their vector:

$$\left\{ \begin{array}{l} \text{Central} : C_{m\alpha}|_i = \frac{C_m|_{i+1} - C_m|_{i-1}}{\alpha|_{i+1} - \alpha|_{i-1}} \\ \text{Ends} : C_{m\alpha}|_i = \frac{C_m|_{i+1/i} - C_m|_{i/i-1}}{\alpha|_{i+1/i} - \alpha|_{i/i-1}} \end{array} \right. \quad (4.8)$$

and the results will be displayed in the following section. Along with $C_{m\alpha}$ values from simulations, database values were also computed, treated in the same way to preserve consistency.

4.1.1 Static analyses

To pursue our goals, steady computations must be run at every single angle of attack. In Tab.4.1 are summarised the options selected to set the analyses.

Static Stability Numerical Set-Up	
<i>Time configuration</i>	Steady
<i>Iterations</i>	2000
<i>Mathematical flow model</i>	NS, Turbulent
<i>Numerical scheme</i>	Central, 2nd order accuracy
<i>CFL</i>	2
<i>Turbulence Model</i>	SA/BL

Table 4.1. Static Analyses Numerical Setting.

Pitching moment coefficients, and static stability derivatives are then extracted as shown in Tab. 4.1.1. Since, as mentioned previously, there is a problem in reaching perfect convergence, an arbitrary choice has been made to find the following results: taking time history of oscillations, the last 400 iterations values have been collected and then averaged.

	0°	5°	10°	20°	30°
C_m	-0,0005	-0,0194	-0,0339	-0,0618	-0,0849
<i>Database</i>	0	-0,0272	-0,0366	-0,0564	-0,0758
$C_{m\alpha}$	-0,0038	-0,0033	-0,0028	-0,0026	-0,0023

Table 4.2. Computed and database values of static pitching moment coefficient at different angles, and, in the bottom row, the rate $C_{m\alpha}$.

Those values are then reported on respective graphs to better render the results' trend (Fig.4.1 and Fig.4.2).

As can be noticed, comforting results have been obtained: their trend respects the one given from the experimental database employed for comparison and validation, with some discrepancies that range from 5 to 15% using Baldwin-Lomax model for turbulence computation, with a run time of approximately 7 hours for every 2000 iterations with 2 processors available for computing.

Unfortunately, those cannot be considered yet as valuable results, since errors can be negligible only if minor than 5%, but for what may concern the generic stability of the capsule, it is well approximated, and, therefore, may be used as a preliminary design tool.

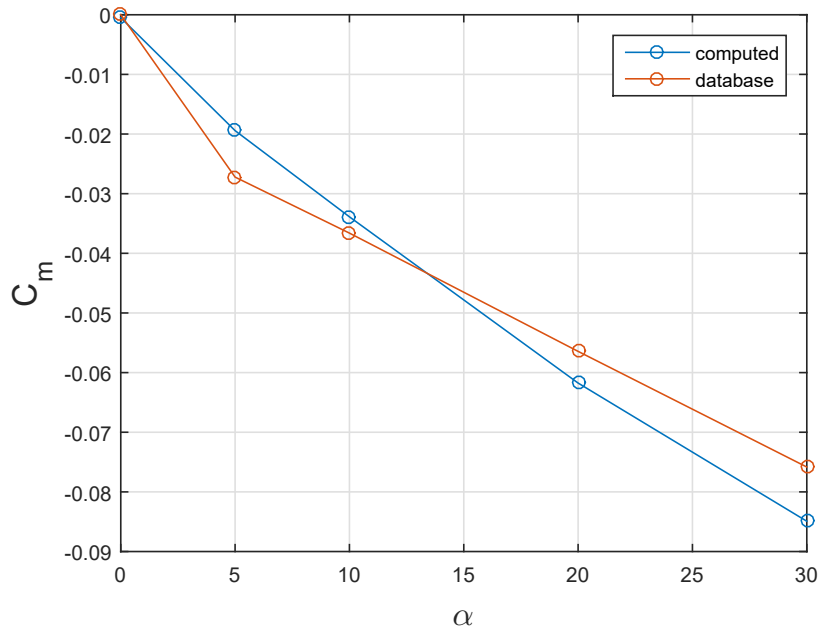


Figure 4.1. Pitching moment coefficients at fixed angles of attack.

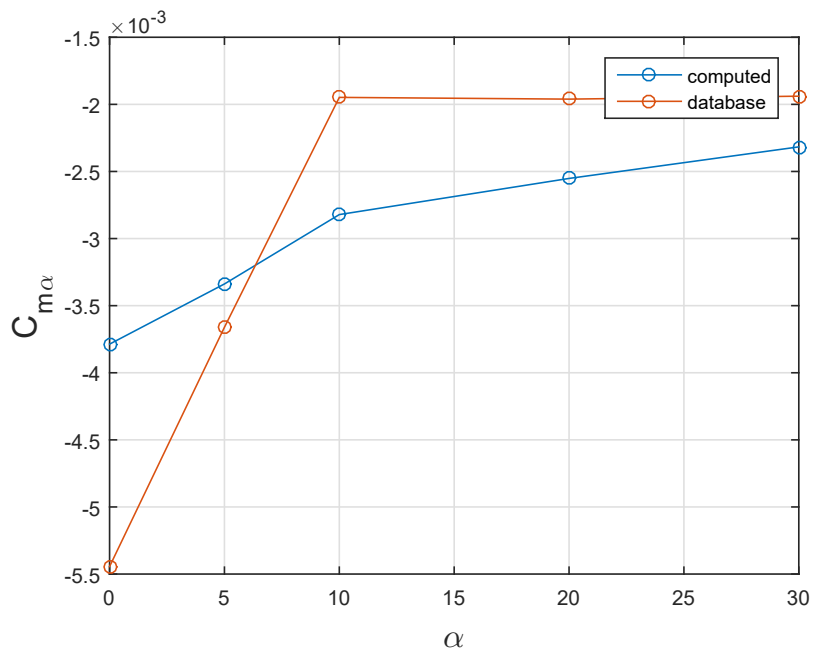


Figure 4.2. Static derivative values over the angles of attack range analysed.

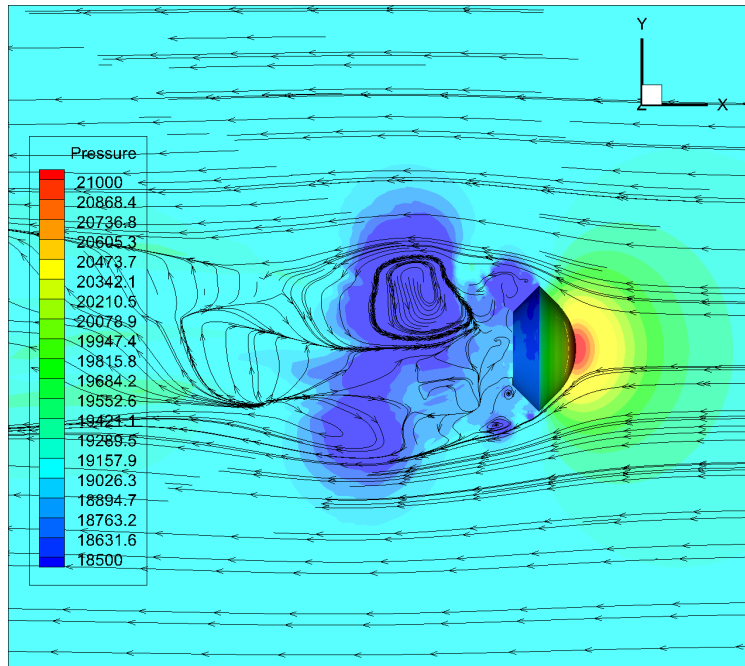


Figure 4.3. Capsule at $\alpha = 0^\circ$ - Flow visualisation (BL turbulence model).

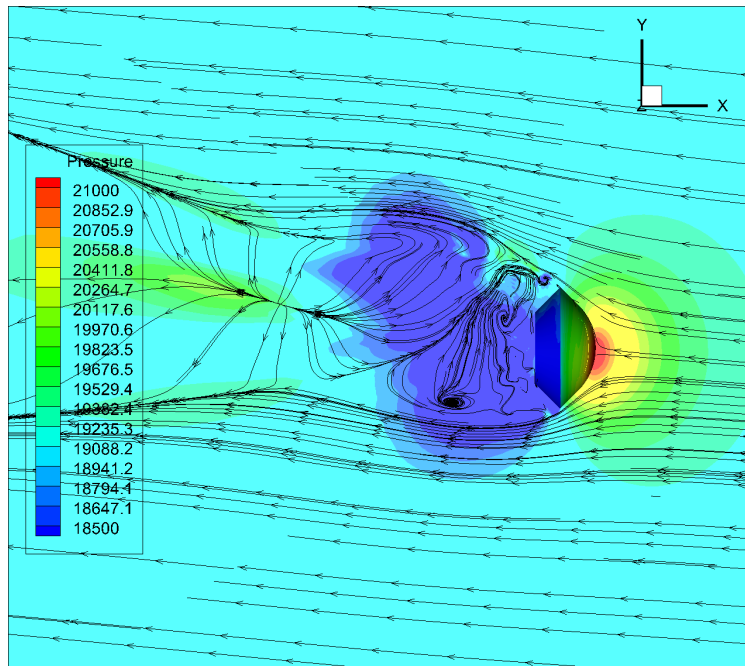


Figure 4.4. Capsule at $\alpha = 5^\circ$ - Flow visualisation (BL turbulence model).

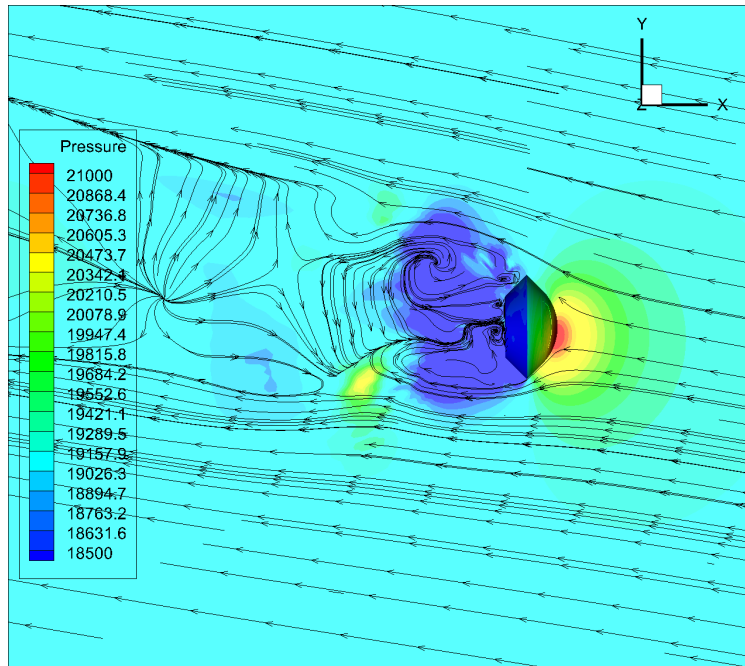


Figure 4.5. Capsule at $\alpha = 10^\circ$ - Flow visualisation (BL turbulence model).

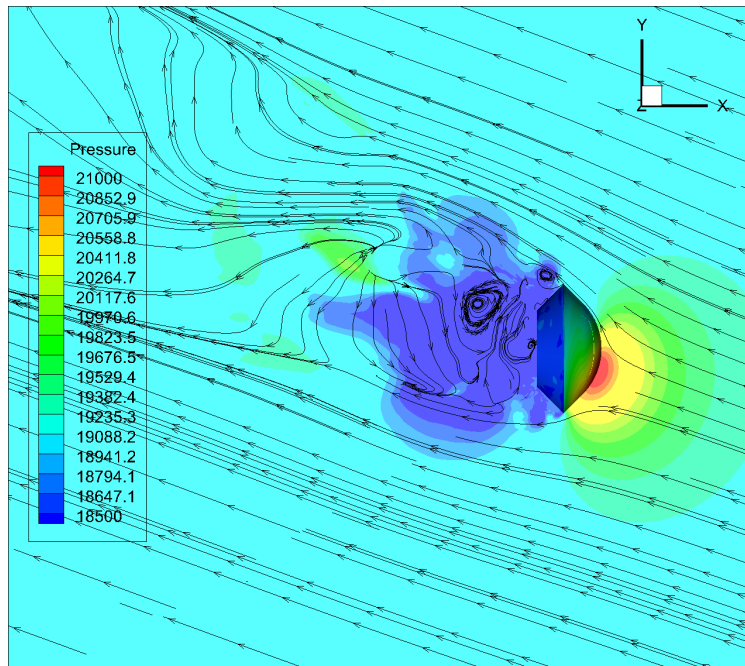


Figure 4.6. Capsule at $\alpha = 20^\circ$ - Flow visualisation (BL turbulence model).

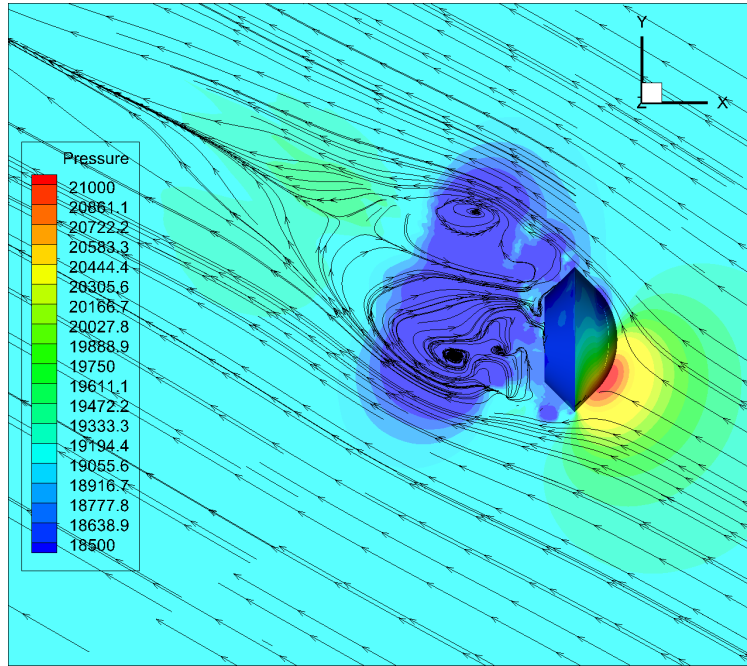


Figure 4.7. Capsule at $\alpha = 30^\circ$ - Flow visualisation (BL turbulence model).

Computation of C_N and C_A

As the database available gives informations also on axial and normal acting forces, and as the software in use computes forces and moments on the specified body, an auxiliary computation of these other two coefficients is performed, as it can be useful to further validate the presented model.

As seen before, for pitching moment, coefficients may be extracted as in Eq.4.9 and Eq.4.10.

$$C_N = \frac{N}{\frac{1}{2}\rho_0 V^2 S} \quad (4.9)$$

$$C_A = \frac{A}{\frac{1}{2}\rho_0 V^2 S} \quad (4.10)$$

and these results are then compared with experimental ones as displayed in Fig.4.8 and Fig.4.9.

As one may notice, in the normal coefficient trend, the same error as in pitching moment one is still present. A much more negative impact is instead visible in axial coefficient, where the trend is comparable, but there is an offset between the curves, whose reason may be the flow resolution in the wake region. In fact, drag strongly depends on how the body affects the zone behind it, in terms of velocity profiles: the more the velocity defects, the larger the force will be [38].

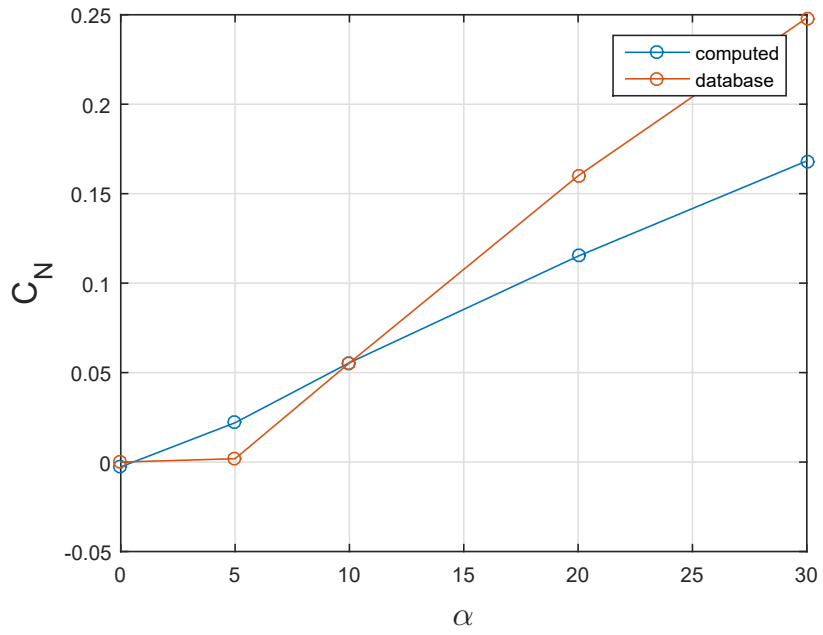


Figure 4.8. Normal force coefficients at different angles of attack.

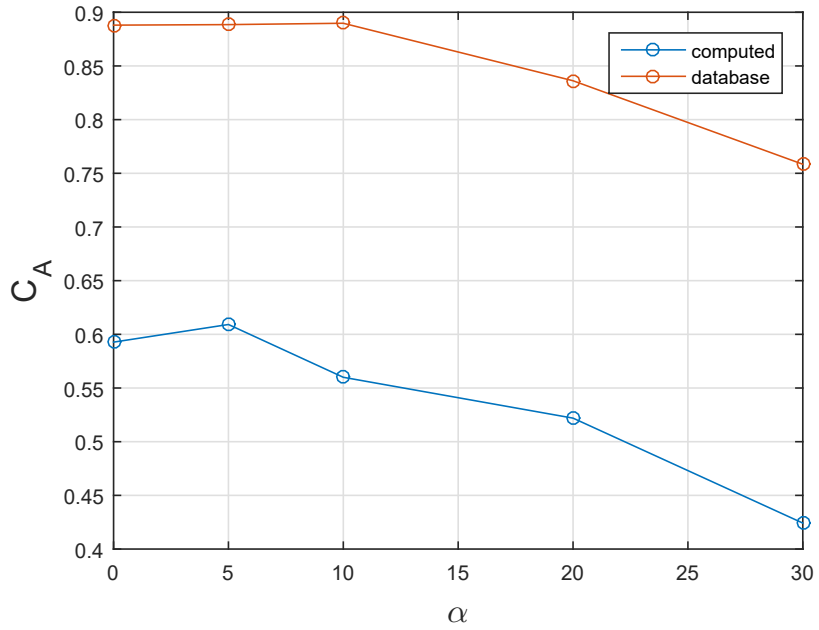


Figure 4.9. Axial force coefficients at different angles of attack.

An idea to better clarify this point could be performing accurate computations with particular attention to the wake, refining the local grid and choosing an appropriate turbulence model.

Errors

To be exhaustive, here are displayed percentual errors for every computation between computed and database solution.

Those are calculated as in Eq. 4.11:

$$err = \frac{|(X_{computed} - X_{database})|}{X_{database}} 100 \quad (4.11)$$

with the exception of values near 0 degrees, where axial force and pitching moment approach to zero. In those cases, error reaches unreasonable high values, and its computation is therefore changed into Eq. 4.12.

$$err \approx |(X_{computed} - X_{database})| 100 \quad (4.12)$$

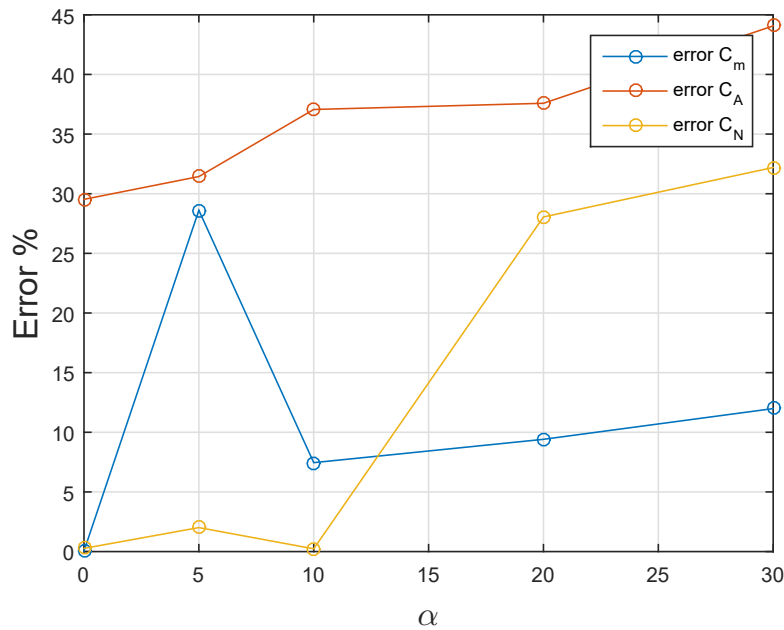


Figure 4.10. Errors in % for axial, normal forces and pitching moment coefficients, at various angles of attack.

The most accurate computation proves to be the one about the pitching moment, even if at 5 degrees there are still some large uncertainties, while drag error is strongly affected by the mentioned offset.

Those hints must be taken into account in further developments of this study.

4.2 Dynamic Stability

Dynamic stability evaluation is currently an unsolved problem for modern flight mechanics of reentry vehicles: it is hard to evaluate and to quantify, and since different models have been developed, different approaches can be used.

What's more, different terms can be assumed as indicative of the dynamic behaviour of a body: usually, pitching moment can be expressed as the sum of different terms, each of them responsible of the different items affecting the phenomenon (Eq.4.13) [19].

$$C_m = C_{m0} + C_{m\alpha}(\alpha - \alpha_0) + C_{m\dot{\alpha}}\dot{\alpha} + C_{mq}q + C_{m\dot{q}}\dot{q} \quad (4.13)$$

Influences are mainly caused by pitching motion (speed and acceleration) and variation of angle of attack.

Usually, dynamic stability information is identifiable in C_{mq} alone, or in a so defined "*damping sum*" which takes into account the angle of attack variation: $C_{m\dot{\alpha}} + C_{mq}$, and each time will be explained what term we will be referring to. The difference between the two is an essential assumption, but their meaning is the same: in one case, pitch angular speed is hypothesized to be *equal* to incidence variation rate, in the second case they're *separate* terms.

In this work, two main approaches will be used, and then compared, to see which gets closer to the database at disposal.

From a numerical point of view, to discover the capsule's dynamic response to a fixed-amplitude disturbance, forced oscillation technique will be employed and discussed in the following sections.

4.2.1 Forced Oscillation Technique

There are different ways for performing analyses of dynamic stability, both experimental and analytical. The most used and efficient methods are essentially three [30]:

1. Free oscillations: a model is held in a fixed position on a sting that permits free oscillatory motion, either damping down or growing, based on the dynamic stability inherent in the model geometry;
2. Forced oscillations: similar to the previous method, the model here is forced through a prescribed oscillatory motion, and damping can therefore explicitly be determined. It can be also used to predict limit cycle oscillations in flight;
3. 6-DOF analyses: this is essentially a scaled flight test, reproducing points of the object's trajectory. In fact, it decomposes the rigid body motion into a

translation of the center of mass and a rotation about the axis located at the same point [33];

Although the free oscillation method has several features that can make experimentation and simulation processes easier [40], simplicity and direct computation are some of the many reasons that can lead to the choice of forced oscillation technique as analysis mean: based on the principle of "oscillating the aircraft model around its center of gravity with small and constant amplitude oscillations in a single degree of freedom"[31], the relationship between the aerodynamic forces and the primary motion in the plane of motion is established. Oscillating the model in different degrees of freedom yields various dynamic stability derivatives that can be therefore investigated.

Oscillations are only performed on the plane of symmetry described by axes X-Y (Fig.4.11).

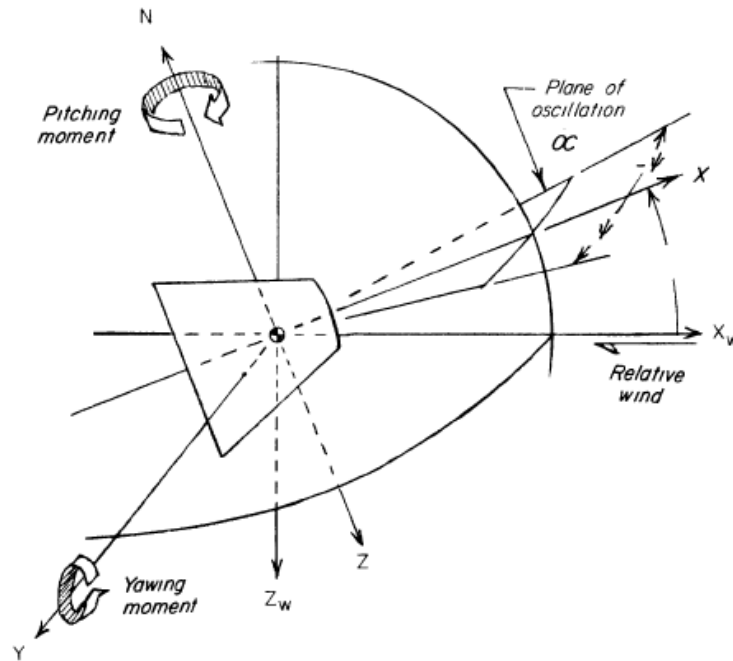


Figure 4.11. Identification of oscillations in reference system [32].

The extraction of the desired dynamic derivatives is rather a complex process for experimental analyses: the same result can be more easily pursued by the use of CFD, with NS based equations that can more accurately predict those derivatives [33]. That, of course, has to deal with the fact that measuring loads can be extremely hard experimentally, instead can be easily predicted numerically, and

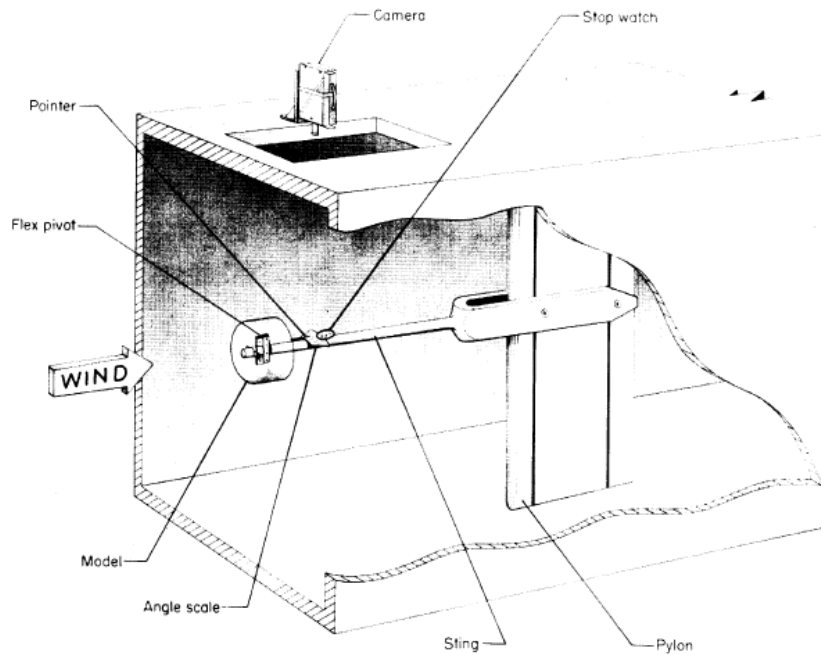


Figure 4.12. Typical experimental setting for oscillating body analyses (*Langley stability tunnel*) [32].

time histories for each one can be easily recorded.

Further evaluation of the time histories of forces and moments can be made in different ways, and that defines the different methods with which one may approach the problem. The ones that will be employed in this study are:

- Fourier harmonics comparison
- Angular velocity maximum and minimum evaluation

and that will be fully described in next sections.

Of course other methods exist and have been elaborated by experts, but these were chosen for their simplicity and capability to be better employed with the available outputs, to better focus on the validation of the CFD model and procedure.

The oscillating motion that will be imposed on the body has a sinusoidal pattern, and so will be the body response' shape, that can be usually expressed as in Eq.4.14 and represented as in Fig.4.13 as example:

$$\theta = \alpha_0 + A \sin(\omega t + \phi) \quad (4.14)$$

Of course, the response can be lagged by a phase ϕ that depends generally from the body inertia, that measures its reactivity to an impulse.

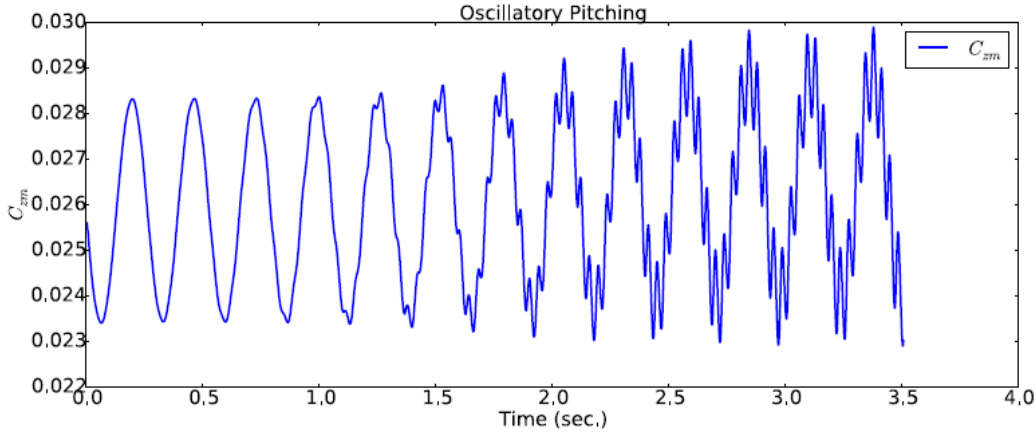


Figure 4.13. Body response to forced sinusoidal oscillation (*Orion Crew Module CFD simulation*) [19].

Fourier harmonics comparison

Once time histories of the interested loads are got, one approach could involve the transfer from time-domain to frequency-domain via Fourier analysis [36].

This consists in the identification of two main parts of the response itself: if the first Fourier harmonics has the expression as shown in Eq. 4.15

$$f(x) = a_0 + a_1 \cos(x\omega) + b_1 \sin(x\omega) \quad (4.15)$$

one may identify a *in-phase* component (sinusoidal), and an *out-of-phase* one (cosinusoidal). Those play different roles in the dynamic behaviour of the body [34]: in particular, pitching moment can be expressed as in Eq. 4.16.

$$M = M_{stat} + M_{sin} \sin(\phi(t)) + M_{cos} \cos(\phi(t)) \quad (4.16)$$

$$\begin{cases} C_{stat} = \frac{M_{stat}}{1/2\rho V^2 SD/2}; \\ C_{sin} = \frac{M_{sin}}{1/2\rho V^2 SD/2}; \\ C_{cos} = \frac{M_{cos}}{1/2\rho V^2 SD/2}; \end{cases} \quad (4.17)$$

Here, one may compute corresponding static, sine and cosine coefficients for pitching moment (Eq. 4.17): the first is a constant, the second (*in-phase* component) produces zero net work on the model over a cycle of the periodic motion, and the third (*out-of-phase* component) plays instead a role in work production on the model. Indeed, it reflects the dynamic response of the body: if negative, the

behaviour will be damped, otherwise a positive value of the out of phase coefficient will mean an enhancement of oscillatory motion.

Cosine and sine coefficients can be obtained fitting the body response time history to Fourier first harmonic, process that can be pursued easily with the aid of the MATLAB function "fit" after having imported the computed data.

Angular velocity maximum and minimum

A simple method, otherwise, could be defined evaluating points of maximum and minimum ω [35]: plotting C_m values obtained from computations versus θ (pitching angle due to oscillatory motion), the figure obtained is shaped as an elliptical hysteresis, where the mentioned two points can be easily identified as lowest and highest points where $\alpha = \alpha_0$, that equals to conditions where is verified that $\theta = 0$ (Fig.4.14).

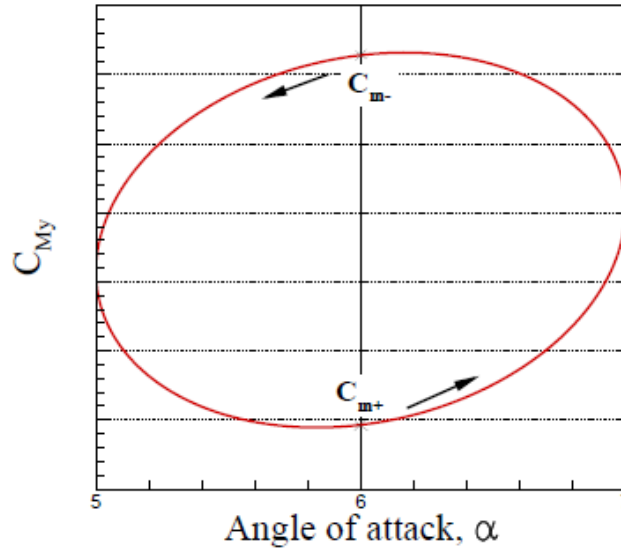


Figure 4.14. Example of body response to forced sinusoidal oscillation: C_m versus α of attack [35].

In those points, the corresponding pitching moment coefficients can be described as in Eq.4.18 shown below:

$$\begin{cases} C_{m+} = C_{m0} + (C_{m\dot{\alpha}} + C_{mq}) \frac{\omega Ac}{2V} \\ C_{m-} = C_{m0} - (C_{m\dot{\alpha}} + C_{mq}) \frac{\omega Ac}{2V} \end{cases} \quad (4.18)$$

from which, subtracting one another, pitching moment can be found as in Eq.4.19:

$$C_{m\dot{\alpha}} + C_{mq} = \frac{C_{m+} - C_{m-}}{2kA} \quad (4.19)$$

where $k = (\omega c)/(2V)$ is called *reduced frequency* and c is the capsule's length in this case ($D/2$).

4.2.2 Dynamic Analyses

To pursue our goals, unsteady computations this time must be run at every single angle of attack. In Tab.4.2.2 are summarised the options selected to set the analyses.

Dynamic Stability Numerical Set-Up	
<i>Time configuration</i>	Unsteady
<i>Global iterations</i>	100
<i>Inner iterations</i>	15
<i>Mathematical flow model</i>	NS, Turbulent
<i>Numerical scheme</i>	Upwind, 1st order accuracy
<i>CFL</i>	0,8
<i>Turbulence Model</i>	SA - Extended Wall Function
<i>Time step</i>	0,0005 s
<i>Frequency</i>	20 Hz
<i>Amplitude (absolute value)</i>	0.017 rad/1°
<i>Initial angle of attack</i>	0, 5, 10, 20, 30 deg
<i>Reduced frequency</i>	0,2244

Table 4.3. Numerical setup for dynamic analyses

This particular setting was chosen because at higher amplitudes of oscillation the flow solver went into strong instabilities that made it stop computing after only eight time steps at best. Higher amplitudes are so a subject to be further investigated.

The reduced frequency employed is similar to the one in the experiments of Hiraki et al. [25], so the phenomenon is presumably the same the database refers to and validation takes place univoquely.

Data concerning stability are extracted thanks to the two methods described before, so that a comparison can be made and informations on their reliability can be easily gained.

Computations have been set with different initial angles of attack, and, for each case, the converged steady computation was set as its initial solution, to avoid extra iterations. Of course, as previously said, even at fixed position the

phenomenon is unsteady, so it is presumable that the very first iterations will be transitory-like.

Grid motion was applied to solid boundaries, so a small displacement can be observed during oscillation cycles as in Fig.4.15-4.16.

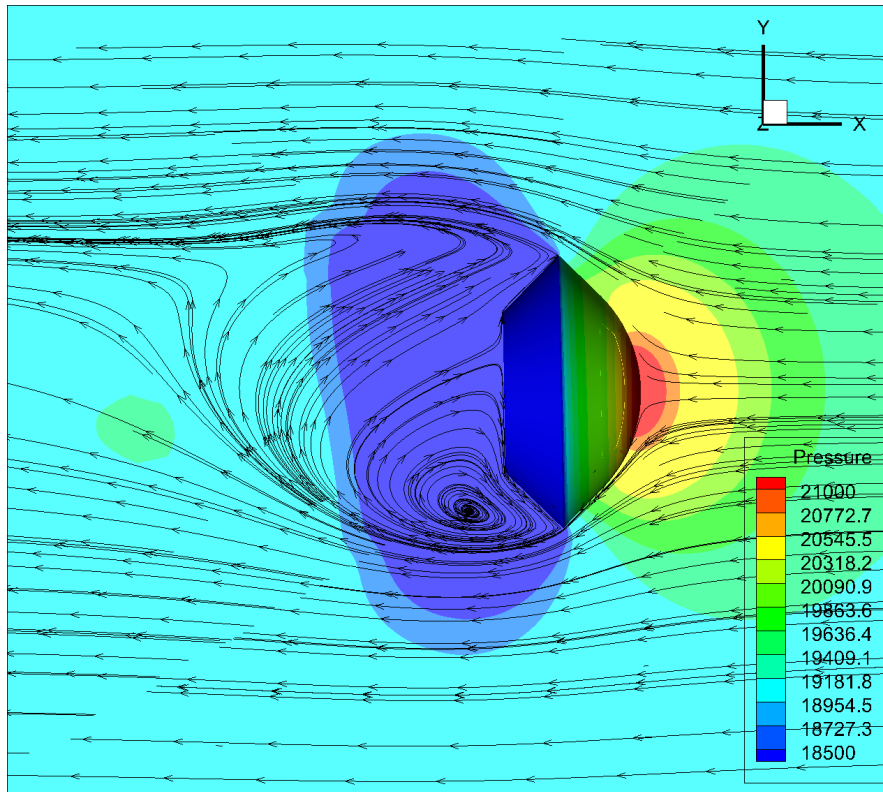


Figure 4.15. Oscillation at $\alpha_0 = 0$: time step at 3/4 of a complete cycle.

Every computation was set to catch at least one complete cycle of forced oscillation motion: every iteration lasted about 30 minutes, making every simulation run for about 2 days to succeed, with 2 processors available for computing.

In Fig. 4.17, 4.18, 4.19, 4.20, 4.21 are displayed pitching moment responses with their respective Fourier series approximation and their input signal (Fig. 4.22). Despite the already cited issues of the present model, simulations gave very smooth oscillations in pitching moment, except the initial transition.

Different behaviours can be perceived at different initial angles of attack:

- At 0 degrees, there is a phase delay of almost 180 degrees between input and response, and the C_m smoothes as time proceeds, but does not faithfully follow the original sinusoidal path;

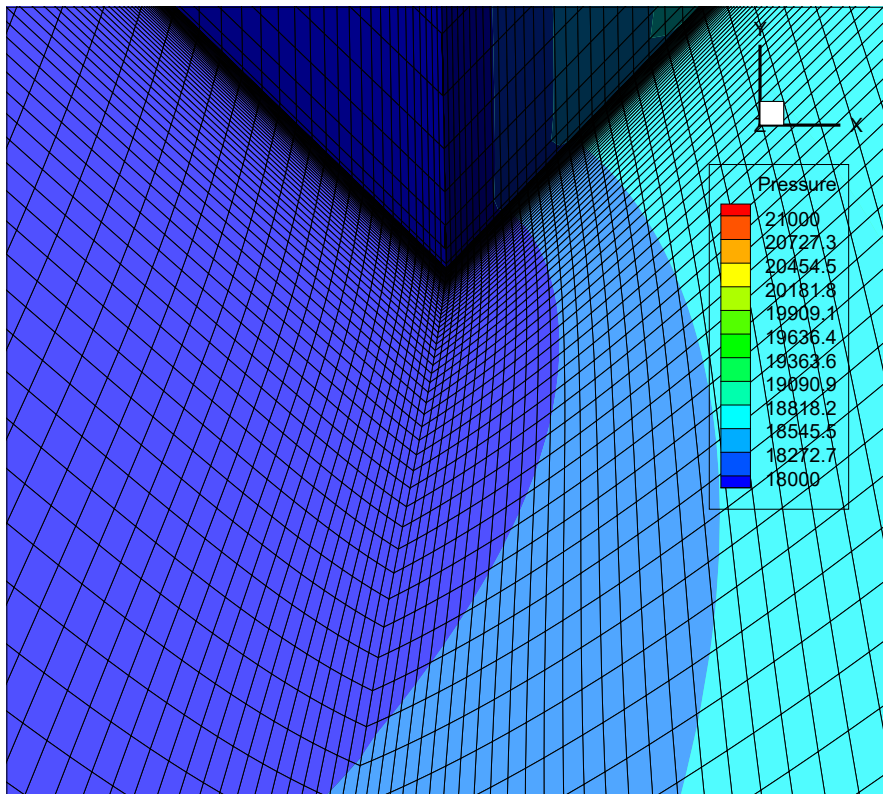


Figure 4.16. Detail of the same time step as Fig.4.15: grid is deformed as the body oscillates.

- At 5 degrees, a phase presence can be highlighted, and again response does not seem to resemble the input motion. Oscillations, indeed, smooth through time;
- At 10 degrees, phase increases, and higher oscillations are present at higher times;
- At 20 degrees, oscillations start to reflect a sinusoid motion (that can be observed by the Fourier harmonic) and again phase rises;
- At 30 degrees, oscillations enlarge during oscillations, and the behaviour is similar to the previous case's one.

Of course, a forced sinusoidal motion will result in a sinusoidally-shaped response from the body. Indeed, as can be seen, this wave-path will be followed differently depending on the initial conditions: from 0 to 30 degrees of angle of attack, pitch coefficient undergoes an increase of number of oscillations around the sine-wave path and also of phase delay from the input wave motion.

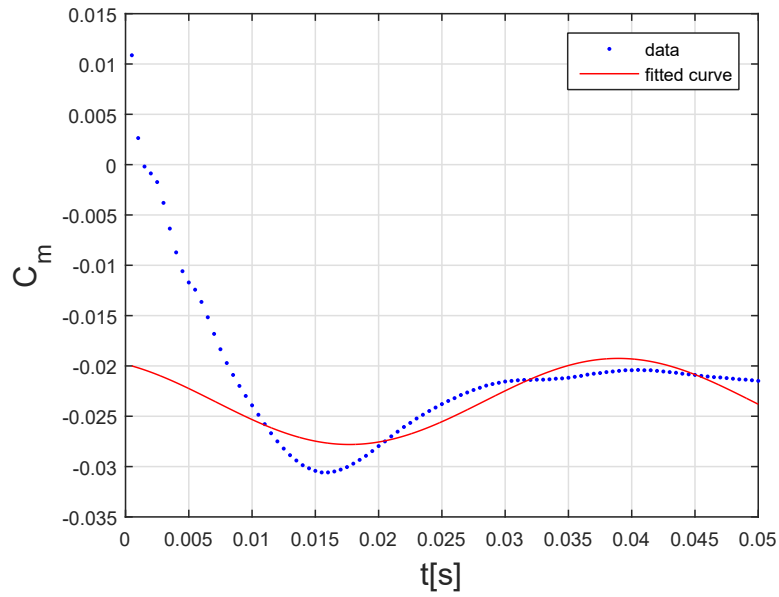


Figure 4.17. Fourier harmonics corresponding to pitching moment oscillation ($\alpha_0=0^\circ$, $\theta = 1^\circ$).

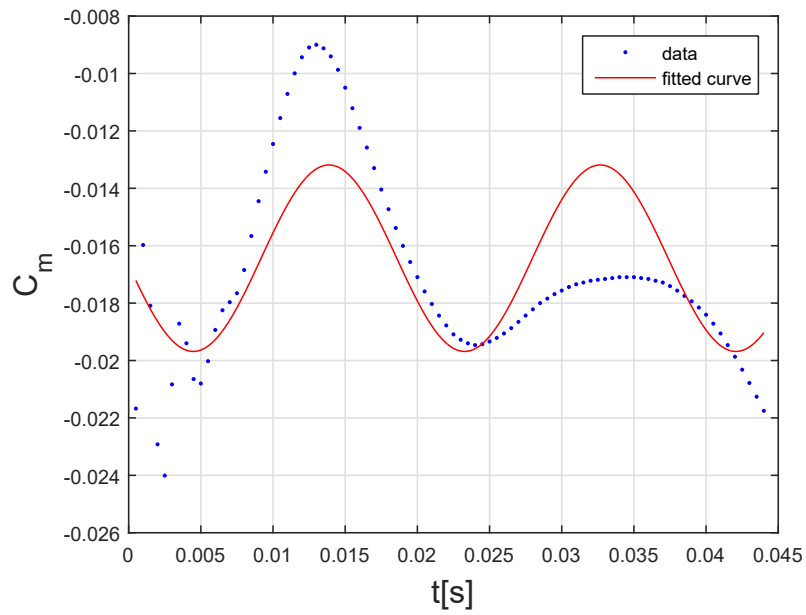


Figure 4.18. Fourier harmonics corresponding to pitching moment oscillation ($\alpha_0=5^\circ$, $\theta = 1^\circ$).

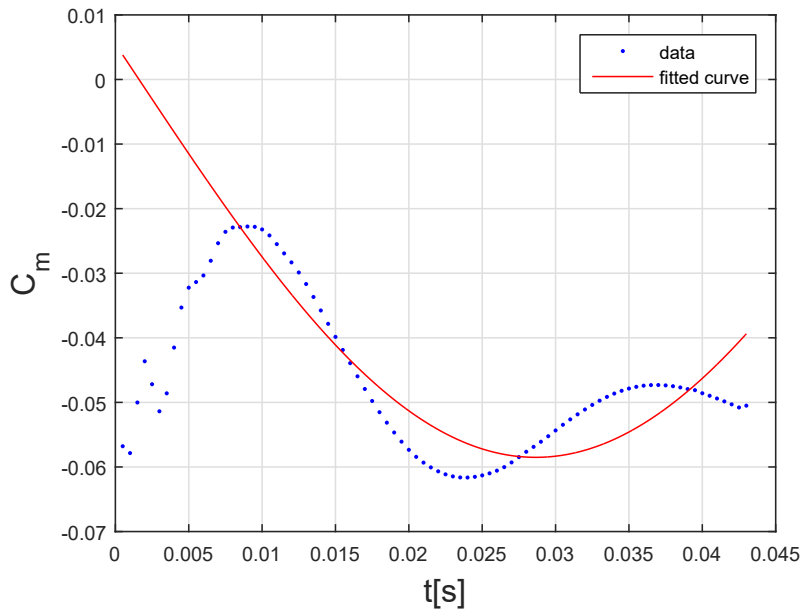


Figure 4.19. Fourier harmonics corresponding to pitching moment oscillation ($\alpha_0=10^\circ$, $\theta = 1^\circ$).

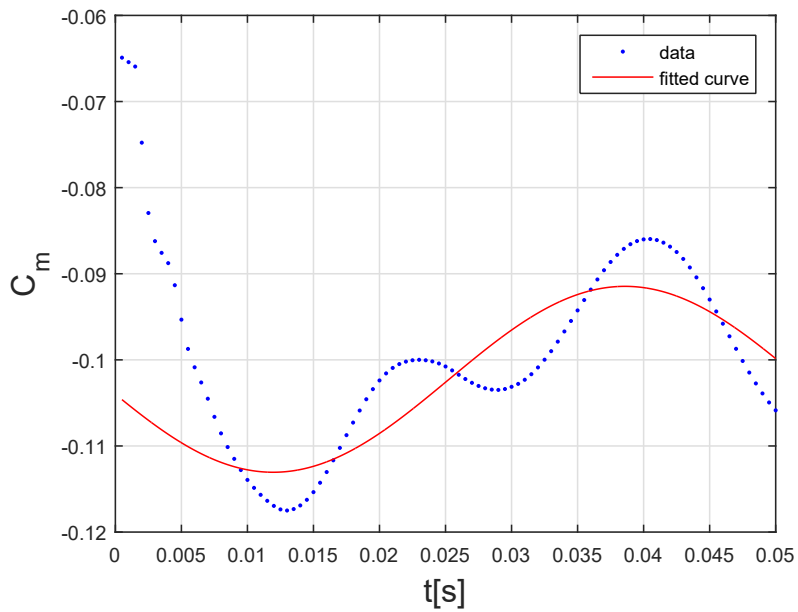


Figure 4.20. Fourier harmonics corresponding to pitching moment oscillation ($\alpha_0=20^\circ$, $\theta = 1^\circ$).

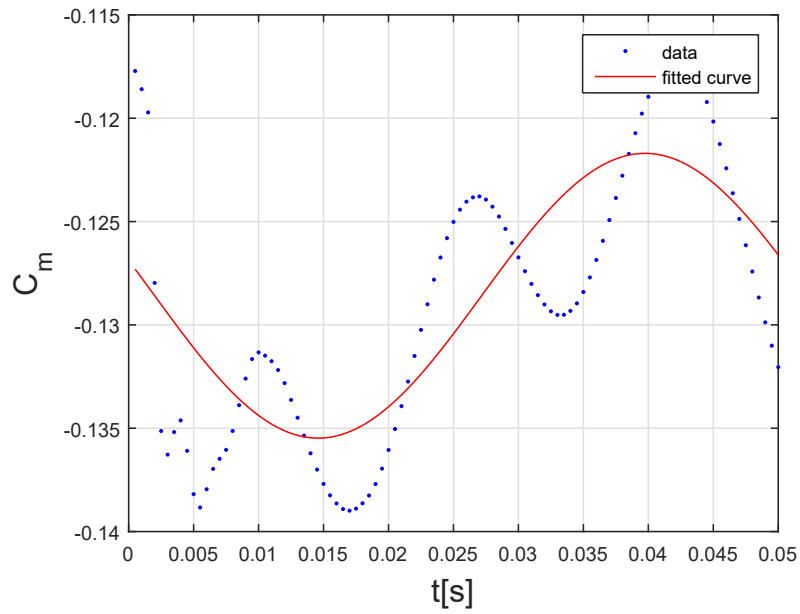


Figure 4.21. Fourier harmonics corresponding to pitching moment oscillation ($\alpha_0=30^\circ$, $\theta = 1^\circ$).

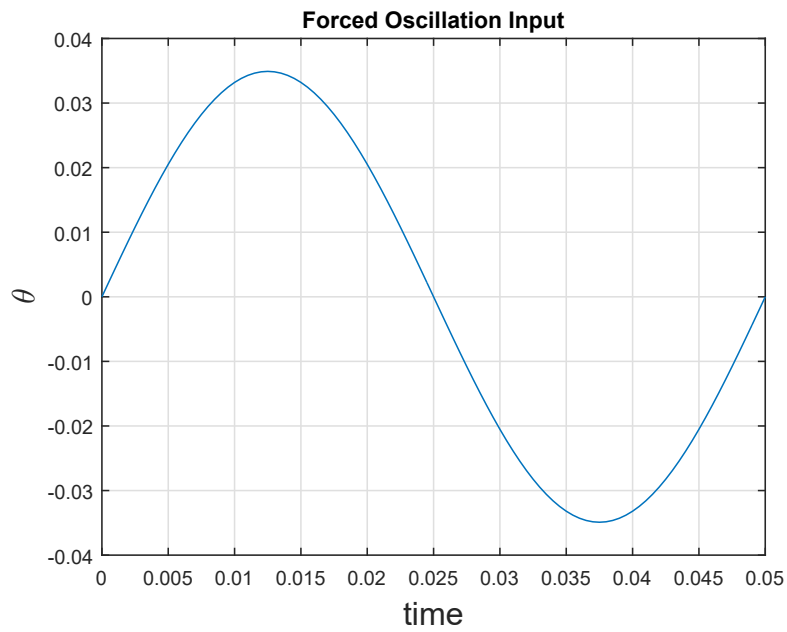


Figure 4.22. Forced sinusoidal oscillation signal input.

So, there are two main features that are highlighted increasing incidence:

- Oscillations around sinusoid;
- Phase lag, which shifts curves leftwards (mostly visible in 0° - 5° - 10° cases)

These can be explained via the mechanism of dynamic stability proposed by Teramoto. In terms of angular speed, plots are displayed in Fig.4.23, 4.23, 4.25, 4.26, 4.27.

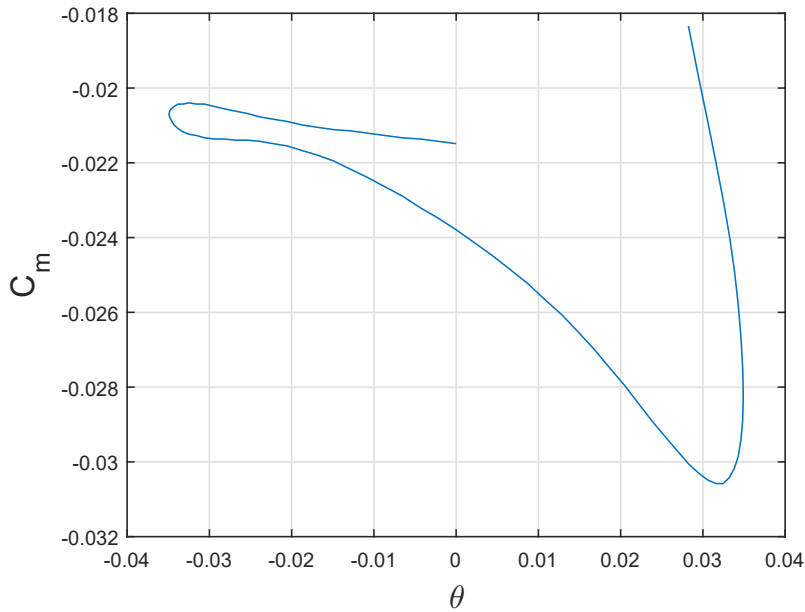


Figure 4.23. Pitching moment coefficient vs Pitching angle ($\alpha_0=0^\circ$, $\theta = 1^\circ$).

Clearly, the initial transient phase emphasizes the body's response: this part must be of course excluded from the discussion that follows (15 initial iterations have been excluded therefore). As can be seen from these plots, instead, a different point of view can be adopted: the range in which pitch angle varies during a cycle is obviously constant as the imposed motion is the same for every initial condition, but curves do not follow a circular path at high angles, because of the mentioned oscillations. There is instead a hysteresis that can be seen as an index of the gap between the two signals, and, therefore, a measure of how much stable the capsule is. Anyway, since only one cycle of oscillation was computed, this model seems to be very dependent on personal discern, so these results will be treated taking this aspect into account.

Numerically, comparing to database values, the results of these two approaches adopted in this work are plotted in Fig. 4.28.

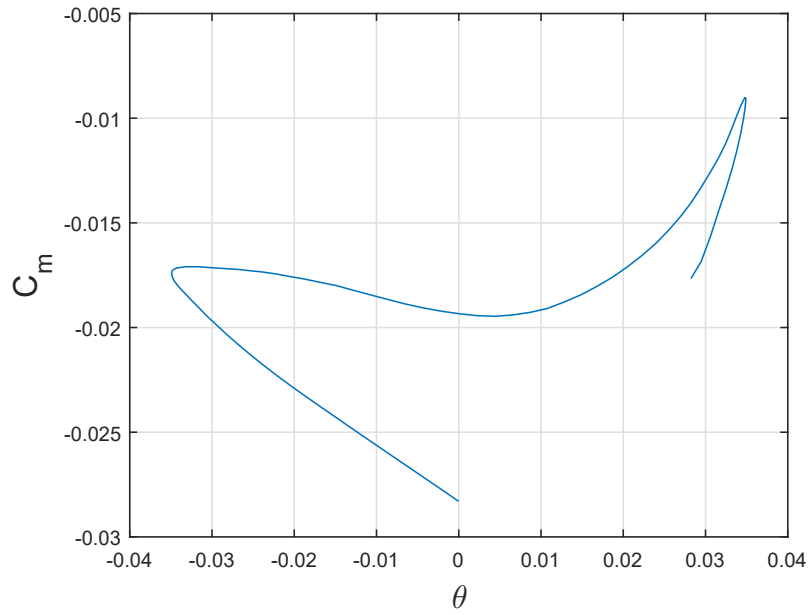


Figure 4.24. Pitching moment coefficient vs Pitching angle ($\alpha_0=5^\circ$, $\theta = 1^\circ$).

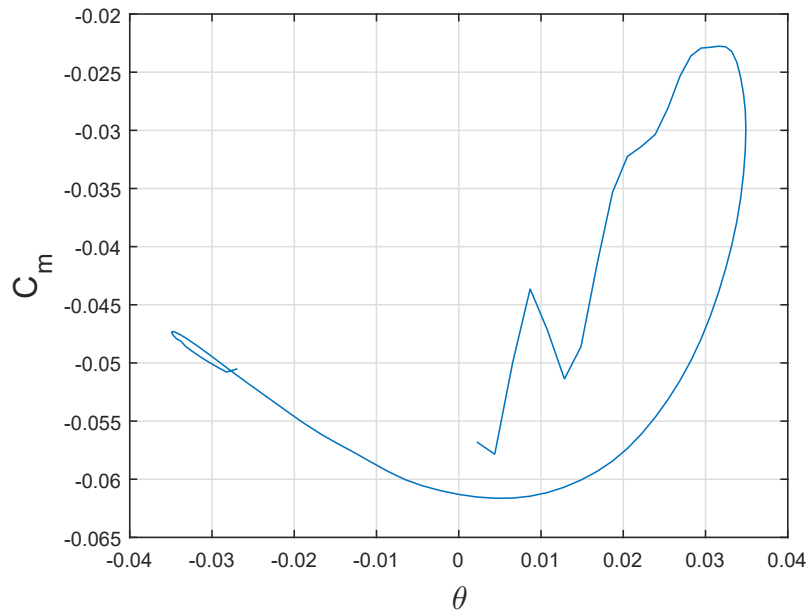


Figure 4.25. Pitching moment coefficient vs Pitching angle ($\alpha_0=10^\circ$, $\theta = 1^\circ$).

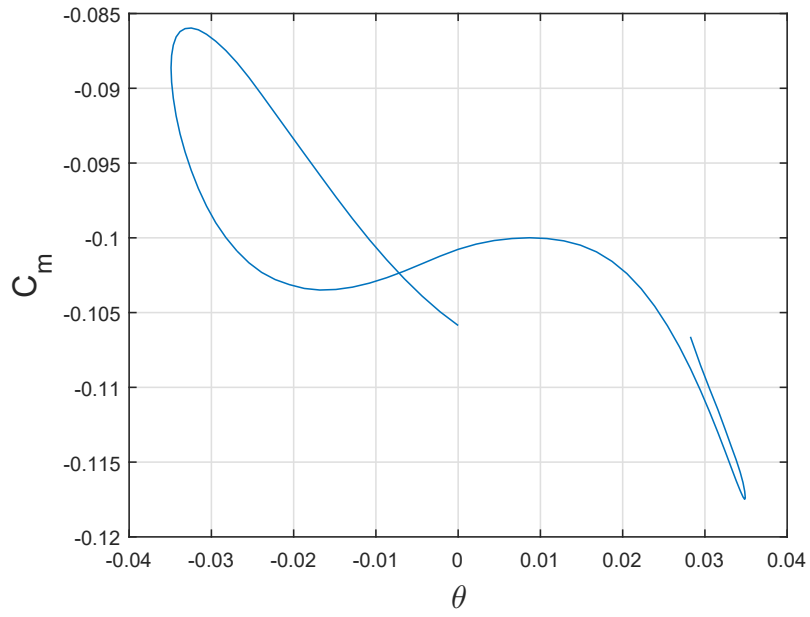


Figure 4.26. Pitching moment coefficient vs Pitching angle ($\alpha_0=20^\circ$, $\theta = 1^\circ$).

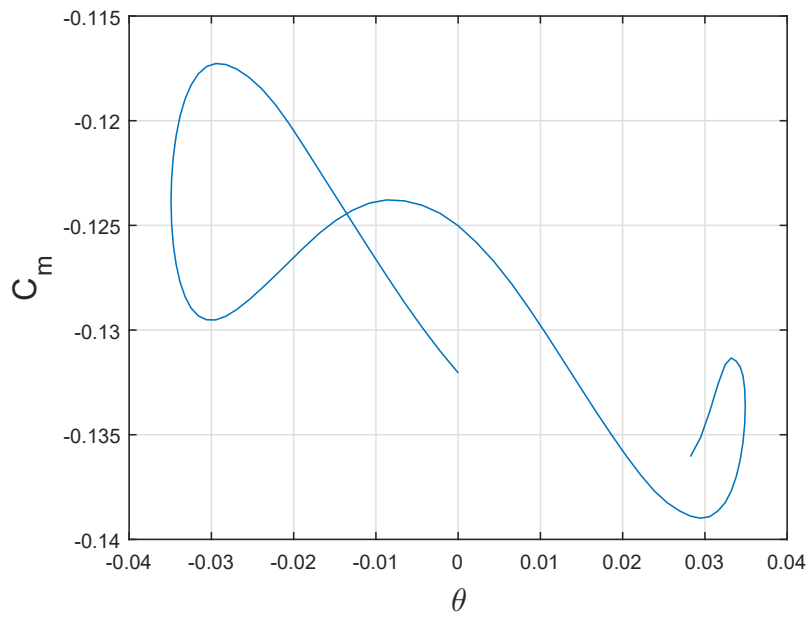


Figure 4.27. Pitching moment coefficient vs Pitching angle ($\alpha_0=30^\circ$, $\theta = 1^\circ$).

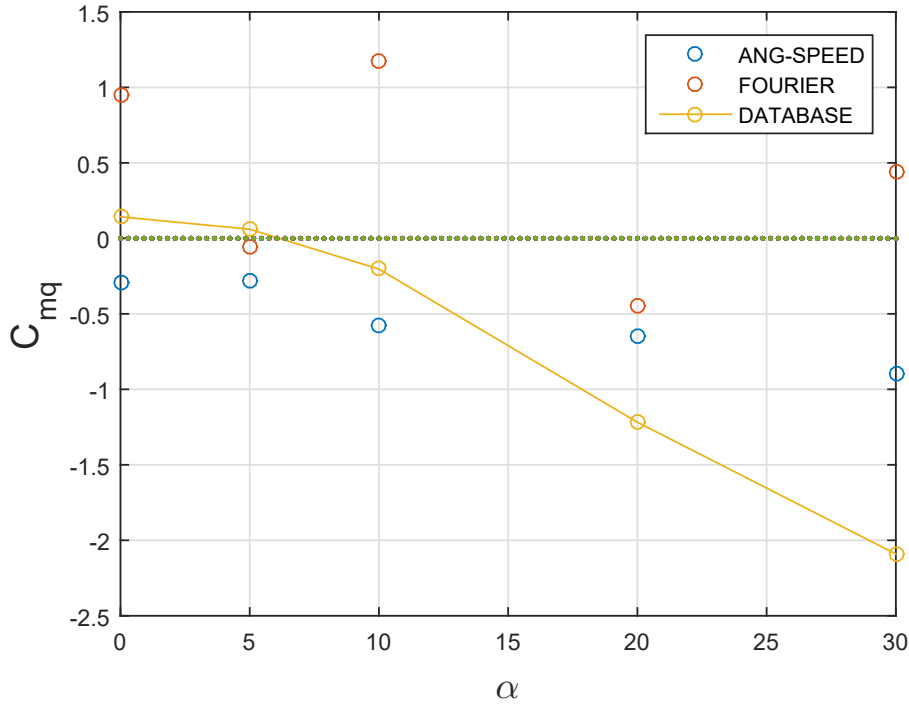


Figure 4.28. Dynamic damping derivative: values computed (Fourier serie and Angular Speed methods) and from available database. Over the green line the capsule has UNSTABLE behaviour, otherwise it is STABLE.

A preface is mandatory: simply by qualitatively evaluating the response obtained, one may reasonably assert that increasing angle of attack seems to be improving stability characteristics. In fact, at higher angles, the capsule motion oscillates around the original imposed path, but stays on track, while at lower angles the sinusoidal movement seems to be completely lost.

Looking now at the summarizing graph of results in Fig. 4.28, the first observation that comes to the eye, is that the conditions at high angles of attack look as issued, since they differ from the database trend.

Secondly, one may notice that the database curve results quite represented by the points computed with the angular speed method, while the one elaborated with Fourier harmonics has the tendency to be conservative, underestimating the capsule' stability, which only occurs at 5° and 20° with this method. Instead, angular speeds' evaluation tends to overestimate this feature, which results always verified.

There are however too few elements to univoquely establish which of the two is the most accurate, and therefore this topic will be needing further investigation.

Teramoto’s Proposed Dynamic Stability Mechanism

It is interesting to focus on the physical meaning of the topic just described, that is why it is reported a proposed explanation to this phenomena.

Some main events can be observed [25], and for what concerns the phenomena highlighted in this work:

1. The hysteresis that can be observed in the pitching moment is due to the delay of base pressure (where *base* stands for the capsule’s back).
2. There is an oscillation in static pressure, and a delay that is strongly dependant on the recirculating region behind the capsule, and the possible compression shock wave, if present.

Teramoto et al.[25] proposed a phenomenological description of dynamic stability, that unfolds as follows:

1. The capsule, while oscillating, propagates its disturbance downstream inside the wake with convection. Since this propagation has a finite speed, a delay is present in the wake.
2. The base pressure is controlled by the flow that stands in the recirculating region, and therefore a delay will be affecting pressure also.
3. This same delay has a second effect exactly on the pitching moment’s hysteresis creation, whose trend is to make the capsule more likely to become unstable.

From results obtained in this work, is possible to assert that a delay in pitching response to forced oscillation is certainly present, and the origin stands in the wake zone, since with angles of attack variation this is the most affected flow region.

Second, the presence of this delay results in an oscillatory behaviour around the input motion: this surely can lead to strong instabilities for much higher angles of attack, since the oscillation amplitude presumably enlarges even more. So, with this data, it is reasonable to say that the proposed mechanism is verified.

It is clear how further cycles computation could be determining in this mechanism’ discovery and understanding, so it would be precious to perform this kind of analyses, along with the same post-processing, that surely would be more accurate. In this thesis, only qualitative evaluations can be truly appreciated.

A further possible development to investigate this particular topic could be measuring pressure for base and front of the capsule, and analyze the phases between the two and the oscillation itself, then comparing the results with more accurate computations of pitching moment values.

Chapter 5

Validating the model: limitations and future works

When it comes to evaluating a method, several aspects must be taken into account, and are therefore hereafter analyzed, to give a global idea of the main features of this work.

Accuracy

Concerning this aspect, some measures have to be applied certainly due to errors that have often been observed among results:

- Increasing grid cells number could surely help resolve some interesting regions (wake, edges, etc.) with proper refinements, and even have better convergence in steady simulations;
- A sting could be attached to the model, to perform a simulation of the full experimental setting, that should affect results mostly at lower speeds [39];
- 2-equation turbulence models can be adopted: $k-\epsilon$ is suggested, for example, in a study on the Orion crew module [19];
- Combined solutions for turbulence models in boundary layer and outer flow could be a chance;
- Computing more oscillation cycles in dynamic motion could help have a better view of the phenomenon;
- Oscillations with different frequencies must be investigated: some papers [36] report an influence of this parameter on the CFD out-of-phase coefficient;

- Since the investigated phenomenon is unsteady, for static stability purposes an idea could be to run unsteady simulations at fixed angle of attack.

Trend prediction capability

Although the previous section underlined certain issues, in every serie of computation that was made, results sticked to the physics of the problem, which is a great result for following improvement.

Indeed, trends for results were always respected and followed, even with a consistant margin of error.

Computational time and efficiency

On the computational side, due to the availability of only 2 processors for running simulations, times were dilatated:

- For steady computations, an average time of 6-7 hours took to run about 2000 iterations and reach a convergent condition;
- For unsteady computations, about two days took to compute one complete cycle of oscillation only.

FINE/TurboTM proved to be a good software for simulation capabilities (i.e. forced oscillation motion tool) and optimization options, but it lacks aerodynamic purposes tool and features, making computational setting sometimes poor or approximated for one's aims. A license with CFL booster is also necessary to perform simulations - especially steady ones - in little times, with strongly stable convergence. In fact, a great limitation in this work was the latter's unavailability, that constrained CFL number to be low.

Topics to further investigate and possible developments

Some main choices have been made at the beginning of this work, but that can make material for further investigations:

- First, this same model should be applied to other configurations of entry capsule to fully understand the true capabilities of this work;
- Only subsonic flow was considered, so one choice could be performing analyses with other flow regimes: in literature, many data are available for supersonic and hypersonic flows, for example. This will be implying a deeper study on grid shape also depending on the shock position (*shock fitting*);

-
- Aerothermal analyses and chemical properties could be combined, since they strongly affect aerodynamics especially in the early stages of the reentry procedure;
 - Dynamic analyses could be conducted with different techniques like the ones mentioned, also experimentally;
 - Other softwares could be employed, with different peculiarities, different numerical schemes available, different moving grid capabilities, etc: a comparison of the two could be clarifying and interesting;
 - Pressure of base and front of the capsule could be included among the measured variables, and then used to compute dynamic coefficients and properties [25] (using the lag of phase between pressure signal and the input one).

These are only ideas that could give future life to this work.

Chapter 6

Conclusions

This thesis had the purpose to build a procedure to effectively analyse a generic capsule' stability during reentry.

Indeed, this model has several issues that are worth attention in more detailed investigations, since they strongly affect results, even if the capability of predicting trends can be positively assessed. Some key elements in the whole procedure play substantial roles and are here summarised.

Grid dimensions are worth paying attention to, even if with accurate choices and analyses setup one may limit the number of cells, obtaining satisfying results. Furthermore, since the recirculation region in the wake is an important part of the whole phenomenology, the choice of the appropriate turbulence model surely makes the difference when it comes to faithfully represent what occurs: for this matters, Spalart-Allmaras is the advised model to adopt, at slightly higher computational costs.

The unsteadiness of the flow, both in static and dynamic simulations, has proven to be the key fact that determines the blunt body's behaviour: in static cases, the two main vortexes that coexist in the wake - in particular their asymmetry - affect the pitching motion. In dynamic cases, the phase lag present between the static pressure of front and back of the capsule determines the response to a forced sinusoidal input. Of course, unsteady simulations, for these reasons, are preferred in any simulation.

For dynamic purposes, there is still a lot to discover: different methods can lead to results more or less valuable and a connection must be found. What's more, the methods employed in coefficients extraction proved to be a valid auxiliary tool in this work, but the gained results are yet too few to truly establish which is the best.

Forced oscillations have expressed their potential through this work, strongly simplifying experimentation, that can be therefore used once the right setup has been found. It should be interesting to investigate other methodologies to fully

understand their capabilities related to this specific topic, and then choose the one that suits the purposes the most. Along, different capsules can be analysed to satisfy the expectations that one may have on a valuable method.

Anyway, hopeful results have been found, in accordance with the available database and with the reported phenomenologies presented by some experts of this subject as Teramoto, and this work can be therefore considered as a good starting point to develop a strongly efficient method: restrictive hypotheses have been made at the beginning, and the present method must be therefore made capable of adapting to more complex situations.

Experimental studies would be also important to be conducted in parallel on different capsules and in different external conditions to successfully confirm the gained data and give more reliability to them and to this model itself.

*"Mankind's greatest achievements have come about by talking, and its greatest failures by not talking. It doesn't have to be like this. Our greatest hopes could become reality in the future. With the technology at our disposal, the possibilities are unbounded. All we need to do is make sure we **keep talking.**"*

Stephen Hawking, 1942-2018

Appendices

Appendix A

MATLAB Script

```
1 clear all
2 close all
3 clc
4
5 %%% DYNAMIC STABILITY DERIVATIVES CALCULATOR %%%
6
7 % Different models are to be evaluated: I hope I'll
  be able to test them out for this specific case.
8
9
10 %%% TEST CASE: HAYABUSA CAPSULE RE ENTRY DYNAMIC
    STABILITY:
11
12 ... from CFD analyses run in Numeca FineTurbo, two
    results types are obtained: 1. STATIC ANALYSES: we
    would be glad to get some static moment coefficients,
    at fixed pitch angle; 2. DYNAMIC ANALYSES: applying
    forced oscillations to the model (variable pitch
    angle, sinusoidal motion) we'd rather get dynamic
    coefficients.
13
14 ... Our assumptions are to stay in subsonic regime of
    motion (last part of reentry), to have an
    axisymmetric shape to deal with, and only PITCH
    MOTION is to be analyzed, negligning every other plane
    of motion.
15
```

```

16
17 Cmq = zeros(1,5)
18 DS_as = zeros(1,5)
19
20 %%%%%%%%%%%%%%%%%%%%%%%%%%%%%%%%%%%%%%%%%%%%%%%%%%%%%%%%%%%%%%%%%%%%%%%%%
21
22 %% STATIC DATA MANIPULATION
23
24 ... As output to our static analyses, we obtain Moment
    values [Nm], at fixed pitch angles.
25 ... These can be directly converted to coefficients
    through simple operations.
26
27 %% DATA
28
29 V = 112;                %m/s, free stream speed
30 alpha = [0 5 10 20 30]; %vector of angles used in deg
31 rho = 0.32;            %kg/m3
32 D = 0.4;                %m diameter = surface(D^2)
33 cref= 0.2;             %m capsule length
34
35 for i =1:5
36
37     Vx(i) = V*(cosd(alpha(i)));
38     Vy(i) = V*(sind(alpha(i)));
39
40 end
41
42
43 q = 0.5*rho*V^2*D^3;    %dynamic pressure*D^2*D
44
45
46 %Moment data
47
48 %values for Pitch Moment
49 Mp = [-0.016 -0.624 -1.088 -1.983 -2.727];
50 %last 400 iter
51
52 Cm = 4*Mp./q           %
    computed

```

```

53 Cm_th = [0 -0.02722 -0.03661 -0.05644 -0.07583] %
    theoretical
54
55 for i =1:5
56
57     if i == 1
58         Cma(i) = (Cm(i+1)-Cm(i))/(alpha(i+1)-alpha(i));
59     else if i == 5
60         Cma(i) = (Cm(i)-Cm(i-1))/(alpha(i)-alpha(i-1));
61     else
62         Cma(i) = (Cm(i+1)-Cm(i-1))/(alpha(i+1)-alpha(i-1));
63     end
64 end
65
66 end
67
68 for i =1:5
69
70     if i == 1
71         Cmath(i) = (Cm_th(i+1)-Cm_th(i))/(alpha(i+1)-alpha(i));
72     else if i == 5
73         Cmath(i) = (Cm_th(i)-Cm_th(i-1))/(alpha(i)-alpha(i-1));
74     else
75         Cmath(i) = (Cm_th(i+1)-Cm_th(i-1))/(alpha(i+1)-alpha(i-1));
76     end
77 end
78
79 end
80
81
82 figure
83 %plot(1:30, plt)
84 plot(alpha, Cma, '-o', alpha, Cmath, '-o')
85 ylabel('C_{m\alpha}', 'fontsize', 16)

```

```
86 xlabel('\alpha','fontsize',16)
87 legend('computed','database')
88
89 %Plotting
90
91 figure
92 plot(alpha, Cm, '-o', alpha, Cm_th, '-o')
93 ylabel('C_m','fontsize',16)
94 xlabel('\alpha','fontsize',16)
95 legend('computed','database','fontsize',16)
96
97 %saveas(figure, 'cm.png')
98
99 err1 = abs((Cm_th-Cm)./Cm_th)*100;
100 err1(1) = abs(Cm_th(1)-Cm(1))*100;
101
102
103
104 %% ADDITIONAL COEFFICIENTS
105 ... Normal and Axial forces
106
107
108 % vector of axial forces [N]
109 A = [95.173 97.81 89.915 83.804 68.110];
110 Ca = 2*A./q*D
111 Ca_th = [0.88801 0.8885 0.889765 0.836204 0.758438];
112 ... second value extrapolated, not given
113
114 err2 = abs((Ca_th-Ca)./Ca_th)*100;
115 err2(1) = abs(Ca_th(1)-Ca(1))*100;
116
117 %vector of normal forces [N]
118 N = [-0.429 3.53 8.916 18.480 27.021];
119 Cn = 2*N./q*D
120 Cn_th = [0 0.0018792 0.055401 0.15997 0.248219];
121
122 err3 = abs((Cn_th-Cn)./Cn_th)*100;
123 err3(1) = abs(Cn_th(1)-Cn(1))*100;
124 err3(2) = abs(Cn_th(2)-Cn(2))*100;
125
```

```

126 figure
127 plot(alpha, Ca, '-o', alpha, Ca_th, '-o')
128 xlabel('\alpha', 'fontsize',16)
129 ylabel('C_A', 'fontsize',16)
130 legend('computed','database', 'fontsize',16)
131
132
133 figure
134 plot(alpha, Cn, '-o', alpha, Cn_th, '-o')
135 xlabel('\alpha', 'fontsize',16)
136 ylabel('C_N', 'fontsize',16)
137 legend('computed','database', 'fontsize',16)
138 %saveas(figure, 'cn.png')
139
140 figure
141 plot(alpha, err1, '-o')
142 hold on
143 plot(alpha, err2, '-o')
144 hold on
145 plot(alpha, err3, '-o')
146 legend('error C_m', 'error C_A', 'error C_N')
147 xlabel('\alpha', 'fontsize',16)
148 ylabel('Error %', 'fontsize',16)
149 %saveas(figure, 'errors.png')
150
151 %%%%%%%%%%%%%%%%%%%%%%%%%%%%%%%%%%%%%%%%%%%%%%%%%%%%%%%%%%%%%%%%%%%%%%%%%
152
153 %% DYNAMIC INPUT MOTION
154
155 ... As before, we get moment values [Nm], but this time,
      their shape is sinusoidal as the forced oscillation,
      presumably with some time/amplitude lag.
156
157 ... We can think of Cm as a composition of terms: Cm0,
      Cma(a-a0),Cmad(ad), Cm(q), Cm(qd).
158 ... Also, we must consider the composition of the
      sinusoidal wave we're imposing on the capsule.
159
160
161 thetaA = 1*pi*2/180;           %amplitude [rad]

```

```

162 theta0 = 0*2*pi/180;           %zero-value
163 N = 1;                         %periods number
164 f = 20;                         %frequency [Hz]
165
166 omega = 2*pi*f;                 %depends on freq
167 k = 2*pi*f*cref/(2*V)           %reduced
    frequency
168 t = [0:0.0005:1/f];             %time vector
169 theta = thetaA*sin(omega*t)+theta0; %angles vector
170
171 figure
172 plot(t,theta)
173 xlabel('time')
174 ylabel('\theta')
175 title('Forced Oscillation Input')
176
177
178
179
180 %% MATLAB COMPUTATION AND FITTING TO FOURIER FIRST
    HARMONICS
181 ... SOURCE: Guidelines for Computing Longitudinal
    Dynamic Stability Characteristics of a Subsonic
    Transport
182
183 ... In this case, interpolation directly through Fourier
    harmonics fitting is performed in such a way:
184 ...  $f(x) = a_0 + a_1 \cos(x*w) + b_1 \sin(x*w)$ 
185
186 %-----ODEG
187
188 filename = fullfile(pwd,'0_deg.txt');
189 fileID = fopen('0_deg.txt','r');
190 A = fscanf(fileID,'%f\n');
191 fclose(fileID);
192
193 time = t(2:length(t))';
194
195 Md = A;
196 Cmd0 = 4*Md/q;

```

```

197
198 f = fit(time(15:length(time)), Cmd0(15:length(Cmd0)), '
      fourier1')
199 figure
200 plot(f,time,Cmd0)
201 xlabel('t[s]', 'fontsize',16)
202 ylabel('C_m', 'fontsize',16)
203 coeff = coeffvalues(f)
204
205
206 % Damping sum - cosine contribution (out of phase)
207 ... IT IS EFFECTIVE AS DAMPING IF IT IS NEGATIVE
208
209 Cmq(1) = coeff(2)/thetaA/k
210
211 % Sine contribution (in-phase)
212
213 Cmalpha(1) = coeff(3)/thetaA
214
215
216 %SAME PROCEDURE FOR OTHER ANGLES
217
218
219 %% ANGULAR SPEED VALUES EVALUATION
220 ... SOURCE: CFD Calculation of Stability and Control
      Derivatives for Ram-Air Parachutes
221
222 ... With this method, angular speeds are taken into
      account: it can have both a maximum and minimum value
      , respectively when alpha = alpha0 in forced
      oscillation motion (+/- omegaA/(2V)).
223
224 %-----ODEG
225
226 Theta = theta(2:length(theta)); %modified vector (no 0)
227 figure
228 plot(Theta(15:length(Theta)), Cmd0(15:length(Cmd0)))
229 xlabel('\theta', 'fontsize',16)
230 ylabel('C_m', 'fontsize',16)
231

```


Bibliography

- [1] Peter A.Gnoffo *Planetary Entry Gas Dynamics*, Annual Review Fluid Mechanics, 1999.
- [2] JAXA, *Asteroid Explorer Hayabusa*, Press kit document, downloaded in November 2017 from official site.
- [3] Nobuaki Ishii, Koju Hiraki, Tetsuya Yamada, Yoshifumi Inatani, Masahisa Honda, *System Description and Reentry Operation Scenario of MUSES-C Reentry Capsule*, The Institute of Space and Astronautical Science, Report SP No.17, March 2003.
- [4] Patrick Gallais, *Atmospheric Re-Entry Vehicle Mechanics*, Springer-Verlag Berlin Heidelberg 2007.
- [5] Pasquale Sforza, *Manned Spacecraft Design Principles*, Elsevier Inc., 2016.
- [6] Cole D. Kazemba, Robert D. Braun, Ian G. Clark, Mark Schoenenberger, *Survey of Blunt Body Supersonic Dynamic Stability*, Journal of Spacecraft and Rockets, 2016.
- [7] Susumu Teramoto, *Computational Study on the Dynamic Stability of a Blunt Re-Entry Capsule at Transonic Speeds*, The Institute of Space and Aeronautical Science, 2000.
- [8] Alan M. Cassel, Michael W. Winter, Gary A. Allen Jr., Jay H. Grinstead, Manny E. Antimisiaris, James Albers, Peter Jenniskens, *Hayabusa Re-entry: Trajectory Analysis and Observation Mission Design*, uploaded on www.researchgate.com by M.W.Winter, 2015.
- [9] John C. Adams Jr., *Atmospheric Re-Entry*, 2003.
- [10] Nobuaki Ishii, Tetsuya Yamada, Koju Hiraki, Yoshifumi Inatani, *Reentry Motion and Aerodynamics of the MUSES-C Sample Return Capsule*, Transactions of the Japan Society for Aeronautical and Space Sciences, 2008.
- [11] Prasun N. Desai, Robert A. Mitcheltree, F. McNeil Cheatwood, *Sample Return Missions in the coming decade*, 51st International Astronautical Congress, 2-6 Oct Rio De Janeiro, Brazil, 2000.
- [12] Koju Hiraki, Yoshifumi Inatani, *The Aerodynamic Data Base for Asteroid Sample Return Capsule*, The Institute of Space and Aeronautical Science, March 2003.

-
- [13] Masami Sato, Takaya Kobayashi, *A fundamental study of the flow past a circular cylinder using Abaqus/CFD*, SIMULIA Community Conference, 2012.
- [14] D. Charbonnier, J. B. Vos, E. Clopeau, L. Ferracina, L. Marraffa, *MarcoPolo-R ERC Dynamic Stability Characterization: Computational Campaign*, 8th European Symposium on Aerothermodynamics for Space Vehicles, At Lisbon, March 2015.
- [15] Murman S.M., Aftosmis M.J., *Dynamic Simulations of Atmospheric-Entry Capsules*, Journal of Spacecraft and Rockets, Vol. 46, No. 4, July-August 2009.
- [16] Depres D., Tran Ph., *Dynamic instability of reentry space capsules: a numerical investigation*, 6th European Symposium on Aerothermodynamics for Space Vehicles, Versailles, November 2008.
- [17] NUMECA INTERNATIONAL, *FINETM/Turbo Theory Guide*, 2017.
- [18] NUMECA INTERNATIONAL, *IGGTM/Turbo User Guide*, 2017.
- [19] Amarnatha S. Potturi and Oshin Perroomiany, *Dynamic Stability Analysis of the Orion Crew Module through Computational Fluid Dynamics*, 46th AIAA Fluid Dynamics Conference, 13-17 June 2016.
- [20] Jiri Blazek, *Computational Fluid Dynamics: Principles and Applications*, Elsevier Science, 2005.
- [21] B.S. Baldwin, H. Lomax, *Thin Layer Approximation and Algebraic Model for Separated Turbulent Flows*, AIAA 16th Aerospace Sciences Meeting, Huntsville, Alabama, 1978.
- [22] Andrew Nealen, Takeo Igarashi, Olga Sorkine, Marc Alexa, *Laplacian Mesh Optimization*, Proceedings of the 4th international conference on Computer graphics and interactive techniques in Australasia and Southeast Asia, November 29-December 02, 2006, Kuala Lumpur, Malaysia.
- [23] Suzanne M. Shontz, Stephen A. Vavasis, *A Mesh Warping Algorithm base on Weighted Laplacian Smoothing*, Proceedings of the Twelfth International Meshing Roundtable, pp. 147-158 (2003).
- [24] Nobuaki Ishii, Koju Hiraki, Yoshifumi Inatani, *Attitude Motion and Aerodynamic Characteristics of MUSES-C Reentry Capsule*, The Institute of Space and Astronautical Science, March 2003.
- [25] Susumu Teramoto, Kouju Hiraki, Kozo Fujii, *Numerical Analysis of Dynamic Stability of a Reentry Capsule at Transonic Speeds*, AIAA Journal Vol.39, No. 4, April 2001.
- [26] John D. Anderson Jr., *Computational Fluid Dynamics: The Basics with Applications*, McGraw - Hill, 1995.
- [27] O. Karatekin, R. Voets, J-M. Charbonnier, F. Y. Wang, *Incompressible Aerodynamics of a Planetary Entry Capsule*, 18th International Congress on Instrumentation in Aerospace Simulation Facilities, 1999.

-
- [28] Jubaraj Sahu, *Numerical Computations of Dynamic Derivatives of a Finned Projectile using a Time-Accurate CFD Method*, AIAA Atmospheric Flight Mechanics Conference and Exhibit, 20 - 23 August 2007, South Carolina.
- [29] Lars Davidson, *An Introduction to Turbulence Models*, Chalmers University of Technology, Publication n°97/2, September 2017.
- [30] Mark Shoenenberger, Eric M. Queen, *Limit Cycle Analysis Applied to the Oscillation of Decelerating Blunt-Body Entry Vehicles*, RTO-MP-AVT-152, 2008.
- [31] N. Alemdaroglu, I. Iyigiin, M. Altun, F. Quagliotti, G. Guglieri, *Measurements of Dynamic Stability Derivatives using Direct Forced Oscillation Technique*, 19th International Congress on Instrumentation in Aerospace Simulation Facilities, 2001.
- [32] Jacob H. Lichtenstein, Lewis R. Fisher, Stanley H. Scher, George F. Lawrence, *Some Static, Oscillatory, and Free-Body Tests of Blunt Bodies at Low Subsonic Speeds*, NASA Memorandum 2-22-59L, April 1959.
- [33] M. Korfanty, J. Longo, *CFD based Dynamic Analysis of Atmospheric Re-Entry Vehicles*, 2nd International ARA Days, October 21-23, 2008, Arcachon, France.
- [34] S.Y. Cheng, M. Tsubokura, T. Nakashima, Y. Okada, T. Nouzawa, *Numerical quantification of aerodynamic damping on pitching of vehicle-inspired bluff body*, Journal of Fluids and Structures 30 (2012) 188-204.
- [35] Mehdi Ghoreyshi, Keith Bergeron, Andrew L. Lofthouse, Russell M. Cummings, *CFD Calculation of Stability and Control Derivatives for Ram-Air Parachutes*, AIAA Atmospheric Flight Mechanics Conference, January 2016, California.
- [36] Joseph R. Thompson, Neal T. Frink, Patrick C. Murphy, *Guidelines for Computing Longitudinal Dynamic Stability Characteristics of a Subsonic Transport*, AIAA 2010-4819, Draft 6/10/10 @9:50am.
- [37] Mark Shoenenberger, Prasad Kutty, Eric M. Queen, Chris Karlgaard, *The Aerodynamics of Axisymmetric Blunt Bodies Flying at Angle of Attack*, 2014 IEEE Aerospace Conference, Big Sky, MT, March 2014.
- [38] Christopher E. Brennen, *Internet Book of Fluid Dynamics*, [http : //brennen.caltech.edu/fluidbook/](http://brennen.caltech.edu/fluidbook/), last updated October 2006.
- [39] Sy Steinberg, Bob L. Uselton, Paul M. Siemers III, *Viking Pitch Damping Derivatives as Influenced by Support Interference and Test Techniques*, Journal of Spacecraft, Vol. 10, No. 7, July 1973.
- [40] Sébastien Paris, *Final Presentation on Experimental Investigation on Aerodynamic Stability of Capsules in Transonic/Supersonic regime*, Von Karman Institute for Fluid Dynamics, ESA ESTEC presentation, 2010.